AIR POLLUTION CONTROL WITH METAL-ORGANIC FRAMEWORKS (MOFs)

Lappeenranta–Lahti University of Technology LUT

Master’s degree Programme in Chemical Engineering, Master’s thesis

2023

Mandi Teinilä

Examiners: Assistant Professor Nima Rezaei

Professor Eveliina Repo

ABSTRACT

Lappeenranta–Lahti University of Technology LUT

LUT School of Engineering Science

Chemical Engineering

Mandi Teinilä

Air pollution control with metal-organic frameworks (MOFs)

Master's thesis

2023

73 pages, 19 figures and 13 tables

Examiners: Assistant Professor Nima Rezaei

Professor Eveliina Repo

Keywords: air pollution, adsorption, metal-organic framework, MOF, MFM-300

Air pollution causes approximately 7 million deaths annually. The most significant pollutants are NO_2 and SO_2 due to their abundance and effect on human health as well as the environment. Approximately 98% of SO_2 and 85% of NO_2 can be removed with the methods currently in use. Since even the trace amounts of these pollutants can affect the human health and the environment, more efficient methods are needed. One option is to use metal-organic frameworks as adsorbents. They have the potential for very high adsorption capacity, selectivity, and stability for multiple adsorption/desorption cycles due to their highly porous structure and tuneable properties. The drawbacks include the sensitivity for moisture and corrosive gases as well as only a few are possible to produce in the industrial scale.

NO_2 and SO_2 are difficult gases to adsorb due to their corrosive nature and tendency to break the bonds in MOFs. NO_2 can be removed with MOFs such as UiO-66-NH_2, MFM-300(Al), Cu-BTC and Mg-MOF-74. For SO_2 removal there are more MOF options found, such as MIL-101(Cr)-4F(1%), MFM-170, SIFSIX-1-Cu, MFM-300(Al) and MIL-160. The only known MOF suitable for removing both NO_2 and SO_2 efficiently is MFM-300(Al). It remains its stability and its high adsorption capacity and selectivity over CO_2 and N_2 that are abundant in flue gases.

In the experimental part MFM-300(Al) is synthetised with microwave reactor and characterised with BET, SEM and XRD. SO_2 and NO_2 removal is modelled using COMSOL Multiphysics 6.0. Simulations are made in three cases: for a gas containing SO_2, NO_2 and both SO_2 and NO_2 with N_2.

TIIVISTELMÄ

Lappeenrannan–Lahden teknillinen yliopisto LUT

LUT Teknis-luonnontieteellinen

Kemiantekniikka

Mandi Teinilä

Ilmansaasteiden hallinta metalliorgaanisilla rakenteilla (MOF)

Kemiantekniikan diplomityö

2023

73 sivua, 19 kuvaa ja 13 taulukkoa

Tarkastaja(t): Apulaisprofessori Nima Rezaei, Professori Eveliina Repo

Avainsanat: ilmansaasteet, adsorptio, metalliorgaaniset rakenteet, MOF, MFM-300

Ilmansaasteet aiheuttavat noin seitsemän miljoonaa kuolemaa vuosittain. Merkittävimmät ilmansaasteet ovat NO_2 ja SO_2 niiden korkean pitoisuuden ja ympäristöön kohdistuvien vaikutusten vuoksi. Noin 98 % SO_2:sta ja 85 % NO_2:sta voidaan poistaa nykyisillä menetelmillä. Koska vähäisetkin määrät näitä epäpuhtauksia voivat vaikuttaa ihmisten terveyteen ja ympäristöön, tarvitaan tehokkaampia menetelmiä. Yksi vaihtoehtoinen menetelmä on käyttää metalliorgaanisia rakenteita (MOF) adsorbentteina. Niillä on potentiaalia erittäin korkeaan adsorptiokapasiteettiin, selektiivisyyteen ja stabiilisuuteen useissa adsorptio/desorptiojaksoissa niiden erittäin huokoisen rakenteen ja säädettävien ominaisuuksien ansiosta. Haittoja ovat herkkyys kosteudelle ja syövyttäville kaasuille, sekä se, että suurin osa on haastavaa valmistaa teollisessa mittakaavassa.

NO_2 ja SO_2 ovat vaikeasti adsorboitavia kaasuja, koska ne ovat luonteeltaan syövyttäviä ja rikkovat sidoksia MOF:issa. NO_2 voidaan adsorboida muun muassa seuraavilla MOF:lla: UiO-66-NH_2, MFM-300(Al), CU-BTC ja Mg-MOF-74. SO_2 adsorboimiseen löytyy enemmän vaihtoehtoja, kuten MIL-101-(Cr)-4F(1%), MFM-170, SIXSIF-1-Cu, MFM-300(Al) ja MIL-160. Ainoa tunnettu MOF, joka sopii sekä NO_2:n että SO_2:n poistamiseen tehokkaasti, on MFM-300(Al). Se säilyy stabiilina ja sillä on korkea adsorptiokyky ja selektiivisyys typpi- ja rikkioksideille CO_2:een ja N_2:een nähden, joita on runsaasti savukaasuissa.

Kokeellisessa osassa MFM-300(Al) valmistetaan mikroaaltoreaktorilla ja karakterisoidaan BET:llä, SEM:llä ja XRD:llä. Rikkidioksidin ja typpidioksidin adsorptio on mallinnettu COMSOL Multiphysics 6.0:lla. Simulaatioita tehdään kolmessa tapauksessa: savukaasulle, joka sisältää SO_2:ta, NO_2:ta ja kaasulle jossa on SO_2:ta, NO_2:ta ja N_2:ta.

ACKNOWLEDGEMENTS

Research was carried out as part of REACT-EU EAKR project ”A77605: Uuden sukupolven katalyytit ympäristöterveyden edistämiseksi Etelä-Karjalassa”, where Etelä-Karjalan liitto was the main funder.

Thanks are in order for all the great people that have helped me during the process of making this thesis. Special thank you to my supervisor Nima Rezaei for guiding me through the process, giving me much appreciated advice and supporting all the way. Also, thanks for Eveliina Repo for your work as the second supervisor. Daria Givirovskaia, thank you for the help on the experimental part and Parsa Amin, thank you for your help with the simulations. It has been a great pleasure working with you all.

Thank you for the friends in Lappeenranta who became like a second family for me when I arrived in a strange city far from home. Thanks for all the support and love I’ve gotten from you making the journey to graduating filled with laughter and a little bit less stressful.

SYMBOLS AND ABBREVIATIONS

Roman characters

b	adsorption affinity	
c	concentration	[mol/m^3]
$c_{p,max}$	adsorption maximum	[mol/kg]
C_p	heat capacity at constant stress	[J/(kg K)]
d_z	Out-of-Plane thickness	[m]
D	thermal diffusion coefficient	[m^2/s]
k	adsorption model parameter	
k_f	thermal conductivity	[W/(m K)]
K_L	Langmuir constant	[m^3/mol]
n	adsorption model exponential parameter	
p	pressure	[bar, Pa]
p_i	partial pressure	[bar, Pa]
Q	heat source	[W/m^3]
q	heat flux by conduction	[W/m^2]
qm	maximum adsorption capacity	[kg/s]
R	gas constant	[J/kg K]
T	temperature	[ºC, K]
t	time	[s]
u	velocity vector	[m/s]
V	volume	[m^3]
v	specific volume	[m^3/kg]
x	vapour content	

Greek characters

α	incidence angle	[°]
ϵ	bed porosity	
θ	volume fraction	
λ	thermal conductivity	[W/mK]
ρ	density	[kg/m^3]
σ	molecular cross-sectional area	[m^2]
τ	effective diffusivity	

Constants

g	gravitational acceleration 9,81	[m/s]

Dimensionless quantities

Re	Reynolds number

Subscripts

ads	adsorption
b	dry bulk
des	desorption
Fr	Freundlich adsorption model
m	maximum
s	solid
Sips	Sips adsorption model
Toth	Toth adsorption model

Abbreviations

BET	Brunauer, Emmett and Teller adsorption theory
FGD	flue-gas desulphurization
HC-SCR	hydrocarbon selective catalytic reduction
MOF	metal-organic framework
PM	particulate matter
SCR	selective catalytic reduction
SEM	scanning electron microscope
SNCR	selective non-catalytic reduction
TGA	thermogravimetric analysis
XRD	x-ray diffraction

Table of contents

1 Introduction

According to World Health Organization (WHO) air pollution is the single biggest environmental issue threatening the human health. The exposure to air pollution is recognized as a risk factor for different diseases affecting the respiratory, neurological, and cardiovascular systems, causing nearly 7 million deaths yearly and decreasing the number of healthy years of life (WHO 2014). Generating energy with combustion is the greatest source of air pollution. The most significant air pollutants include particulate matter (PM), ozone (O_3), nitrogen oxides (NO_X), sulphur oxides (SO_X) and carbon monoxide (CO) (WHO 2021). Secondary PM is formed in the air by physiochemical reactions where SO_2 and NO_X are transformed. Ground level ozone is formed when NO_X and volatile organic compounds react in the presence of sunlight. Therefore, it can be said that nitrogen oxides and sulphur dioxide are the principal pollutants in the atmosphere due to their direct impacts on human health and environment but also because of the forming of other pollutants (Sun et al. 2014).

It is required to remove these pollutants from flue gases and prevent their emission to the atmosphere. Multiple ways of removing these gases have already been developed (Sun et al. 2014). The most common way of removing SO_X from flue gases is to use wet flue-gas desulfurization, because of the availability of limestone, its simplicity, and its removal efficiency (Han et al. 2019). The most widely used method for NO_X removal is selective catalytic reduction where NO_X is converted to N_2 and water with a catalyst (Sun et al. 2014). There are still problems to overcome, such as the corrosive and reactive properties of NO_2. Other drawbacks in methods based on absorption include the high energy requirements due to the regeneration of the utilized absorbent solutions and solvent loss due to the solution evaporation, and thereby more efficient and flexible methods for air pollutant removal is needed. Even trace amounts of toxic pollutants need to be removed which is not achievable with the conventional methods (Kim 2018).

An emerging method for removing SO_2 and NO_2 is to use adsorption. It can be a promising way of executing the removal since it requires small amount of energy for the adsorbent regeneration, it has quite simple process design and it has less problems with the waste disposal compared to conventional methods. Possible adsorbent materials include porous materials such as activated carbon, zeolites, and metal-organic frameworks (MOFs). MOFs are a class of crystalline materials with extensive porosity that can reach up to 90% of free volume and ultrahigh internal surface areas (over 6 000 m^2/g). MOFs have attracted extensive interest among researchers for adsorption as they are a new promising class of porous materials with exquisite tuneable properties (Kim 2018). The main challenges in gas adsorption with MOFs are finding suitable functionalisation, chemical stability, and reusability. The selected MOF needs to remain its structural stability with the adsorbate gas and possible moisture. Especially the corrosive toxic gases can compromise the stability of the MOF used as adsorbent. NO_2 and SO_2 can affect the coordination bonds between the metal centres and organic ligands, causing a breakdown in the MOF structure (Martinez-Ahumada et al. 2021). There are only a few MOFs available that have good selectivity and adsorption capacities for both SO_2 and NO_2.

Until now, most of the adsorption research using MOFs are concentrated on removing CO_2 (Kim 2018). More research is also needed for the removal of trace amounts of toxic molecules in flue gases. In studies regarding the removal of toxic gases from the flue gas typically only one component is studied at a time. This is why conditions closer to realistic industrial applications need further research. In addition, only a few MOFs could be synthetized in an industrial scale as of now (Martinez-Ahumada et al. 2021). For the removal of both SO_2 and NO_2 the only promising MOF is MFM-300(Al). Compared to the other MOFs capable of removing both SO_2 and NO_2, Mg-MOF-74 and Cu-BTC, it has great chemical and thermal stability with a decomposition temperature of 400 °C and great stability even after multiple adsorption-desorption cycles. The adsorption capacities for SO_2 and NO_2 are 7.1 and 14.1 mmol/g, respectively. It also has great selectivity for SO_2 and NO_2 over CO_2 and N_2 which makes it a feasible option for this study (Han et al. 2018).

This thesis focuses in finding the most promising MOF for SO_2 and NO_2 adsorption, synthesizing and characterizing it and simulating the adsorption of SO_2 and NO_2 with the MOF as an adsorbent. The first part of this thesis is the literature review based on scientific papers followed by the experimental study and the results.

2 Air pollution by NO_2 and SO_2 from flue gas

Air pollution is recognised as the biggest environmental threat to human health. The exposure to air pollution can decrease the number of healthy years and it causes nearly seven million deaths annually. Air pollution is known as a risk factor for different diseases affecting the respiratory, neurological, and cardiovascular systems. While in high-income countries the air quality has improved significantly, it has gotten worse in low- and middle-income countries. The inequities in air quality can be explained with the globalized movement of goods as well as inequality in the emission and air quality standards in different countries (WHO 2021).

There are multiple sources for air pollution. Since the industrialization the anthropogenic emissions have exceeded the natural emissions in importance. Generating energy with combustion is the single major source of air pollution. Primary pollutants are emitted directly by the combustion and secondary pollutants form in the air through different physiochemical processes (WHO 2021). The typical flue gas composition is presented in Table 1.

Table 1. Typical flue gas composition (Scala et al. 2005)

Component	Concentration value
N_2	75–76 % vol
CO_2	9–12 % vol
H_2O	8–10 % vol
O_2	4–8 % vol
SO_2	150–400 ppm
CO	400–1000 ppm
NO_X	100–200 ppm
SO_3	<20 ppm

The most significant air pollutants include particulate matter (PM), ozone (O_3), nitrogen oxides (NO_X), sulphur oxides (SO_X) and carbon monoxide (CO) (WHO 2021). Some of the PM is formed in the air by physiochemical reactions where SO_2 and NO_X are transformed. Ground level ozone is formed when NO_X and volatile organic compounds react in the presence of sunlight. Therefore, it can be said that nitrogen oxides and sulphur dioxide are the principal pollutants in the atmosphere due to their direct impacts on human health and environment but also because of the forming of other pollutants (Sun et al. 2014).

2.1 SO_2

Sulphur dioxide and PM from the fossil fuel combustion have been the main components of air pollution for decades in many parts of the World. Sulphur dioxide occurs from combustion of fossil fuels containing sulphur (WHO 2021). Other sources for SO_2 include industrial processes like the extracting metal from the ore, transportation and heavy pieces of equipment burning fuel with sulphur (Han et al. 2019). When SO_2 is oxidized, sulphurous and sulfuric acids format. When neutralized with ammonia it creates bisulphates and sulphates (WHO 2021).

Since 1990, SO_X levels in the atmosphere have dropped significantly in OECD countries because of pollution control, structural changes in the economy, energy savings, technical progress, and fuel substitution (OECD 2013).

2.2 NO_2

NO_X includes seven different compounds which are NO, NO_2, N_2O, N_2O_2, N_2O_3, N_2O_4 and N_2O_5. The most harmful of human health in air pollution is nitrogen dioxide as it is the most prevalent in the atmosphere. Over half of NO_X emissions are produced by automobiles and approximately 20 % by electric power plants. The rest of the emissions come from industrial boilers, incinerators, steel mills and gas turbines (Han et al. 2019). NO_2 naturally produces from nitric oxides when exposed to air and it is a strong oxidant and with water it produces nitric acid and nitric oxide. Nitrogen dioxide produces a myriad of secondary pollutants through the photochemical reaction sequence that’s initiated by solar-radiation-induced activation of nitrogen oxide resulting in organic, nitrate and sulphate particles that are measured as PM_{10} and $PM_{2.5}$ (WHO 2021).

In addition to the health effects, NO_2 is a notable greenhouse gas since it absorbs visible radiation. As it absorbs the radiation it also affects the impaired atmospheric visibility. It regulates the oxidizing capacity of the free troposphere and is a major contributor determining ozone concentrations in the troposphere since the photolysis of nitrogen dioxide is the main initiator of the photochemical formation of ozone (WHO 2021).

NO_X emissions have decreased slower than SO_X emissions from the levels of 1990 (OECD 2013). The amount of NO_X emissions can be affected by producing less of it and preventing pollution. A way to generate less NO_X is to lower the combustion maximum temperature and fuel residence time by using an excess of air and fuel. Another way of limiting NO_X production is to replace air with pure oxygen gas for the combustion process which prevents nitrogen to work as a reactant or using fuel with very low nitrogen concentration. However, separate NO_X removing processes are still needed since even trace amounts are harmful (Han et al. 2019).

2.3 Air pollution in Finland

Air pollution problems are not evenly distributed across the globe. In developed western countries the air quality is better compared to many developing countries but still in big cities the air quality can be momentarily poor due to the traffic. The air quality in Finland is in top class in global comparison. This is explained by the remote location of Finland, the distance from big cities of Europe, and the relatively low emissions. The most relevant air quality problems in Finland are inversion situations in winter, high dust concentrations in urban areas in spring and long-distance migration episodes (Ilmatieteenlaitos).

The limit value of annual average concentration is 40 $\mu g/m^3$ for NO_2 and 20 $\mu g/m^3$ for SO_2. The air quality in Finland is monitored in about 100 air quality stations. The annual average concentration of SO_2 and NO_2 in Lappeenranta are presented in Figure 1 (Ilmatieteenlaitos).

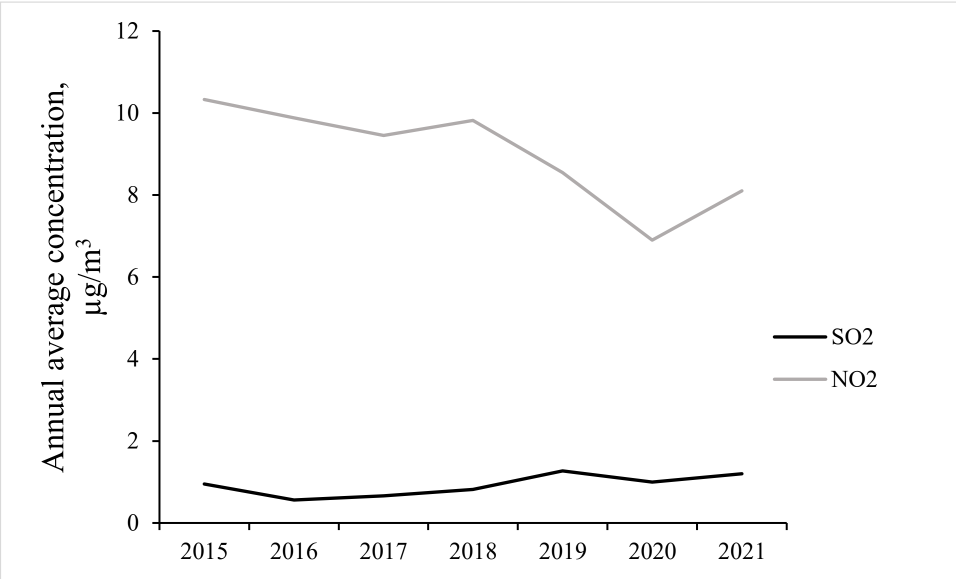

Figure 1. Annual average concentrations of SO_2 and NO_2 in Lappeenranta, Tirilä for 2015–2021 (Ilmatieteenlaitos).

Although Finland's air quality is excellent on a global level, air pollution leads to about 1 500 premature deaths in Finland. NO_2 is typically a problem in bigger cities. In 2015 NO_2 limit values were exceeded only in two air quality stations in Helsinki. So even when the annual limit values are rarely exceeded, health problems are caused by the trace amounts of the pollutants (Vestenius 2016).

3 Removing NO_2 and SO_2 from flue gases

Most of the NO_2 and SO_2 in the atmosphere are emitted for the most part through cars' exhaust fumes and industrial flue gases. It is required to clear these pollutants from flue gases and prevent their emission to the atmosphere. Multiple ways of removing these gases have already been developed and are being used (Sun et al. 2014).

3.1 Conventional methods of removing SO_2

The most common way is to use wet flue-gas desulfurization (WFGD) to remove SO_X from flue gases. It utilizes a slurry with alkaline sorbent such as limestone or lime. (Sun et al. 2014) The adsorption can also be carried out as dry flue gas desulfurization (DFGD), but wet process is the more popular method because of the availability of limestone, its simplicity, and its removal efficiency (Han et al. 2019). Wet limestone FGD processes can remove approximately 92%–98% of the SO_2 from the flue gas. Desulphurization efficiency is controlled by pH range, limestone reactivity, SO_2 concentration, effectiveness of particulate control device, and water recirculation to the scrubber (Gordoba 2015).

In wet FGD, watery sludge containing lime ($Ca(OH)_2$) or limestone ($CaCO_3$) is first sprayed to the upper part of a flue gas scrubber tank. The flue gas containing SO_2 enters the vessel and reacts with the lime or limestone particles which results in the formation of sulphite or sulphate in solid form. Despite the advantages, wet FGD has some issues. It needs an intricated machinery and operation due to the incomplete oxidation of the calcium sulphate which can result in scaling issues. This method also produces a great quantity of solid waste which is typically disposed of in a landfill. The scale of the waste problem is significant as a typical wet scrubber using limestone that processes 680 000 m^3/h flue gas with SO_2 content of 289 kg/h generates 3 729 kg of solid waste every hour and 32 666 t annually (Han et al. 2019). Water is used in vast quantities which need to be treated before releasing back to the environment (Carter et al. 2020).

SO_2 can alternatively be removed using regenerable sorbents in which case the SO_2 can be released and processed into saleable products like sulphuric acid or elemental sulphur. After SO_2 is released, the sorbent can be used again for the adsorption. The most common regenerable method for FGD is called the wet Wellman-Lord process. In this method the SO_2 from flue gas is captured using the equilibrium between sodium sulphite and sodium bisulphite following reaction (r_1) (Han et al. 2019).

$$SO_2 + Na_2SO_3 + H_2O \overset{r_1}{\rightarrow} 2\,NaHSO_3 \tag{1}$$

When heating the process most of the sodium bisulphite that is created after the adsorption can be converted back into sodium sulphite. Therefore, highly effective removal of SO_2 occurs. The advantages of this method include the high removal efficiency and flexibility of product selection. However, the equipment needed is considerably sophisticated and expensive (Han et al. 2019).

To overcome these disadvantages different methods have been developed. In Linde-Solinox process, the chemical reaction follows reaction (r_2).

$$Ca(OH)_2 + SO_2 \xrightarrow{r_2} CaSO_3 + H_2O \tag{2}$$

Magnesium oxide method follows reaction (r_3).

$$Mg(OH)_2 + SO_2 \xrightarrow{r_3} MgSO_3 + H_2O \tag{3}$$

The aqueous ammonia process follows reactions (r_4) and (r_5).

$$SO_2 + 2NH_4OH \xrightarrow{r_4} (NH_4)_2SO_3 + H_2O \tag{4}$$

$$2(NH_4)_2SO_3 + O_2 \xrightarrow{r_5} 2(NH_4)_2SO_4 \tag{5}$$

The common advantages of the wet methods are the great adsorption rate and the high efficiency of the retention of the sorbent. Nonetheless, a lot of energy is needed for the cooling of flue gases before the adsorption and then reheating the sorbent for the gas release. In addition, because handling of the wet sludge is needed the capital costs and operational costs increase (Han et al. 2019).

FGD based dry methods that are regenerable can significantly reduce water and energy consumption since reheating of the gas is not required. It also reduces corrosion hazards, complexity of the design and capital cost due to the dry nature. In the spray-drying process SO_2 reacts in a hot flue stream with sorbent spray that is generated by rotary atomizers. The process follows reaction (r_6).

$$2\ Na_2CO_3 + 0.5\ O_2 + 2\ SO_2 \xrightarrow{r_6} Na_2SO_4 + Na_2SO_3 + 2\ CO_2 \tag{6}$$

This process is now the second most common method of SO_2 removal from flue gas after absorption by wet limestone. (Han et al. 2019) FGD technologies are energy intensive and not effective for deep desulphurization (Cui et al. 2017).

Multiple different dry methods with catalytic oxidation of SO_2 have also been discovered. These methods utilize metal oxides or activated carbon. These methods' effectiveness depends on the capability of contemporaneously act as SO_2 absorbents and catalysts for SO_2 oxidation to SO_3 when O_2 or H_2SO_4 and H_2O is present. When using activated carbon, the specimen source, porosity of the sorbent, the pre-treatment method and surface functionality has a great impact on the absorption capacity of SO_2. Using activated carbon only gives < 5 mmol/g uptake for SO_2 which is over half less than the uptake with more promising materials such as MOFs (Han et al. 2019).

Due to the lack of functional groups and amorphous nature of activated carbon, the research of catalytic SO_2 oxidation in the presence of O_2 and H_2O at the carbon surface is limited to temperature programmed desorption (TPD). This is done using a sequence of reactions where SO_2 and O_2 react and form C-O species with the active site of the carbon sorbent that after that react with SO_2 to form SO_3 and result in regeneration of the active site. However, the loss of carbon occurring during the regeneration because of to the build-up of CO_2 and CO remains as a problem as well as the combustion of activated carbon (Han et al. 2019).

In dry sorbent injection (DSI) powdered sorbent is stirred with water and injected to furnace and economizer with temperatures of 1 000 ºC and 500–570 ºC respectively. The dry sorbent then reacts with SO_2 producing waste product that is gathered in, for example, bag filter. This technique has advances in more affordable capital and operating costs compared to FGD, requires less water and has easy installation. However, the SO_X reduction capacity is low, as it is only capable to remove 50% of the SO_x contamination (Asghar et al. 2021).

One example of the pre-combustion desulfurization methods would be the bio-desulfurization technique. This technique involves three steps which are dissolving SO_2 containing flue gas into water, transforming it to sulphates and reducing to S^{2-} ions under anaerobic environment through bacteria consuming sulphates and finally back to S in aerobic conditions. This method is cost effective since raw material consumption is reduced and in addition to that the sulfur products attain financial advantages. The energy consumption can be maintained low since the method works in atmospheric pressure and ambient temperatures (Zhang 2018). This method is not yet applicable in industrial scale due to its low solid ratio which decreases process efficiency (Çelik et al. 2019).

The common methods of removing SO_2 and the reduction capacities are presented in Table 2.

Table 2. Reduction capacities of different SO_X abatement methods (Asghar et al. 2021)

Removal method	SO_X reduction capacity, (%)
Physical cleaning or pre-combustion removal	30–50
WFDG[1]	80–98
Chemical and biological cleaning	90
Dry sorbent injection	50

[1]Wet flue gas desulfurization

It is necessary to develop more efficient, reversible, and flexible methods to remove pollutants from flue gas since trace amounts are still left with these methods. (Han et al. 2019) Methods based on absorption have multiple drawbacks including the high energy requirements due to the regeneration of the utilized absorbent solutions and solvent loss due to the solution evaporation (Kim 2018). Another common drawback with SO_2 removal is the irreversible reaction between SO_2 and the absorbent (Pacciani et al. 2011). Although up to 98% of SO_2 can be removed from the flue gas as much as 400 ppm can remain. This amount poses noticeable risks for human health and environment (Subcommittee on Acute Exposure Guideline Levels 2000).

3.2 Conventional methods of removing NO_2

The three main methods of preventing NO_X emissions include chemical reduction of NO_X, oxidation of NO_X as well as the oxidation of NO_X after which the product is adsorbed or direct absorption of NO_X using different sorbents (Han et al. 2019). Nitrogen concentration in the fuel can be reduced as well as changing the combustion conditions in a way that minimum possible nitrogen content is achieved (Asghar et al. 2021).

In selective catalytic reduction (SCR) NO_X is converted to N_2 and water with a catalyst (Sun et al. 2014). Ammonia, urea, or hydrocarbons are often used in the process (Han et al. 2019). The reaction mechanism using ammonia follows reactions (r_7) and (r_8) (Asghar et al. 2021).

$$4\,NO + 4\,NH_3 + O_2 \xrightarrow{Catalyst, r_7} 4\,N_2 + 6\,H_2O \tag{7}$$

$$6\,NO_2 + 8\,NH_3 \xrightarrow{Catalyst, r_8} 7\,N_2 + 12\,H_2O \tag{8}$$

Different catalysts have been researched and applied and they often are based on TiO_2-supported V_2O_5-WO and V_2O_5-MoO_3. V_2O_5 is catalytically active even at smaller loadings (<1 %w/w) and WO_3 and MoO_3 act on greater quantities (about 10%). They increase thermal stability of the catalyst while minimizing the loss of surface area and prevent the transformation of TiO_2 from anatase to rutile. TiO_2-anatase is only partially and reversibly sulphated by SO_2 in the exhaust gas which makes it outstanding support compared to other oxides. High catalytic activity is achieved due to the wide dispersion of V_2O_5 on the TiO_2 surface which rise to isolated vanadyl centres (Asghar et al. 2021).

Noble metals, zeolites and activated carbons have been researched besides metal oxides as SCR catalyst. The advantage of zeolites and activated carbons is that they can physisorb NO_2 into the porous structure and at the same time employ as catalysts for their chemical conversion into alternative species containing nitrogen (Han et al. 2019).

This method is definitely the most established and effective method of removing NO_X with destruction or removal efficiency of over 80 %. The disadvantages of SCR process include high initial cost, limited lifespan of the catalyst and issues with ammonia loss with no reaction with NO_X (Han et al. 2019). The ammonia loss is called ammonia slip and that occurs when the unreacted ammonia is vaporized. Unwanted reactions can also limit the NO_X tranformation such as the formation of ammonium nitrate if the operating temperature is lower than 200 ºC (Arsie et al. 2018). These drawbacks can be solved by installing an oxidation catalyst system but that adds to the already high operating cost (Asghar et al. 2021).

The drawbacks in ammonia or urea SCR including freezing, storage space, process complexity and additional costs caused by the urea dosing system, can be overcame with hydrocarbon selective catalytic reduction (HC-SCR). This method uses hydrocarbons instead of ammonia or urea and the reactions follow reactions (r_9) and (r_{10}) (Asghar et al. 2021).

$$NO + HC + 4\ O_2 \xrightarrow{Catalyst, r_9} N_2 + H_2O + CO_2 \tag{9}$$

$$4\ NO + CH_4 \xrightarrow{Catalyst, r_{10}} 2\ N_2 + 2\ H_2O + CO_2 \tag{10}$$

Catalysts used in HC-SCR are ion-exchanged zeolites, noble metal catalysts, and metal oxides. Overall, the common drawback in SCR is the high cost of the catalysts (Asghar et al. 2021).

Selective non-catalytic reduction (SNCR) is a method for NO_X reduction without a catalyst in 900–1000 ºC temperatures. Ammonia and urea are usually used as reducing agents. It's a similar chemical reaction to SCR except for the quite intricate chemistry and free radical reactions. With urea as a reduction agent the reaction follows reaction (r_{11}) (Asghar et al. 2021).

$$H_2NCONH_2 + 2\,NO + \frac{1}{2}O_2 \xrightarrow{r_{11}} 2\,N_2 + H_2O + CO_2 \quad (11)$$

SNCR has more affordable operating cost compared to SCR since no expensive catalysts are used. The efficiency however is significantly lower with a mean efficiency of 55 %. Efficiency depends on the temperature and boiler condition. Typically, temperatures vary from 950 ºC to 1 050 ºC. The desired reaction in reaction (r_{11}) is achieved when the temperature is high enough. If the temperature doesn't reach the desired level, unreacted urea remains, and ammonia slips occur. If the temperature increases over the desired temperature window the reducing agent burns which leads to increased NO_X emissions. SNCR can be utilized over SCR if the standards for NO_X emissions are not strict (Asghar et al. 2021).

Another emerging method of NO_X reduction is using plasma. Plasma is an active species with extensive wide variety of extraordinary characteristics, and it can elevate or catalyse the chemical reaction. It can also combust materials beyond their flammability limits due to the rapid generation of thermally activated species. This is why plasma can be employed in NO_X oxidation to NO_2. Using plasma expands the temperature window and reduces the costs of NO_X reduction (Nguyen et al. 2019). NO_2 reduction capacities of the different methods are presented in Table 3.

Table 3. Reduction capacities of different NO_X abatement methods (Asghar et al. 2021)

Removal method	NO_X reduction capacity, (%)
LNB[1]	35–55
SNCR[2]	30–60
SCR[3]	75–85
SCR with LNB	50–80

[1]Low NO_X burner
[2]Selective non-catalytic reduction
[3]Selective catalytic reduction

Not a single technology is yet optimal for NO_X removal for all combustion systems. An ideal NO_2 capturing would offer high capacity, selectivity and stability and reversibility since NO_2 is a major feedstock for many chemical industries. There are still problems to overcome such as the highly reactive and corrosive nature of NO_2 (Han et al. 2019).

3.3 Removing SO_X and NO_X simultaneously

The simultaneous abatement of SO_X and NO_X would provide high efficiency and economic advantages. One possible method is to use ozone injection and semi-dry chemical process. In the study executed by Yamamoto et al. nonthermal plasma was used for the treatment of flue gases. The removal efficiency of NO_X reached 90% and SO_X 84% (Yamamoto et al. 2016). Xue et al. investigated contemporary removal of NO_X and SO_X using O_3 and NH_3. The removal efficiency of NO_X was 99% and SO_X 88% (Xue et al. 2018). In conclusion, the simultaneous removal of NO_X and SO_X provide higher removal efficiency in a case of single reactor system, and it can generate fertilizers in a form of solid while removing SO_X and NO_X (Yamamoto et al. 2016). Trace amounts of NO_X and SO_X remain so more efficient methods are needed.

4 Adsorption using MOFs

Another option for removing SO_X and NO_X is to use adsorption. It can be a promising way of executing the removal since it requires small amount of energy for the adsorbent regeneration, it has quite simple process design and it has less problems with the waste disposal. Different adsorbents have been tested including silicates, activated carbon, different zeolites, and metal-organic frameworks (MOFs) (Sun et al. 2014).

4.1 Adsorption process

Adsorption takes place in a boundary surface between two substances or phases. The phenomenon responsible of the adsorption are van der Waals or cohesive forces. Adsorption can happen in systems including liquid and gas, solid and liquid, solid and gas or liquid and liquid (Ościk 1982).

Vapours and gases are adsorbed with adsorbents with a highly developed surface. Adsorption can be described as accumulation of the substance in the surface layer. In the case of gas/solid adsorption, there isn’t an actual surface but rather a hypothetical dividing surface called the Gibbs surface which is equivalent to the adsorbent surface. In addition to the Gibbs surface also interfacial surface with two regions is considered. The two regions include the surface layer of the solid adsorbent and the part of the gas phase that is residing in the force field of the adsorbent surface. The number of adsorbed molecules and thus the adsorption capacity is usually displayed with mol (adsorbate)/g (adsorbent) (Ościk 1982).

Adsorption is executed in two different ways; physical adsorption (physisorption) and chemical adsorption (chemisorption). Physisorption is based on the intermolecular forces such as Van der Waals forces and hydrogen bonds and chemisorption in valency forces that are resulted in adsorbent and adsorbate sharing electrons. These adsorption types can be distinguished by the heat of adsorption, reversibility, and thickness of adsorbed layer. In physisorption the adsorption heat is small and large in chemisorption. In case of physisorption the adsorbed substance layer is relatively easy to remove but a chemically adsorbed layer is very hard to remove and requires more drastic measures. Chemical adsorption forms only monolayers whereas physisorption can adsorb a layer with a thickness of several diameters of the adsorbed molecule (Ościk 1982).

4.1.1 Adsorption-desorption isotherm models

According to Brunauer, there are six types of gas and vapor adsorption-desorption isotherms that are presented in Figure 2.

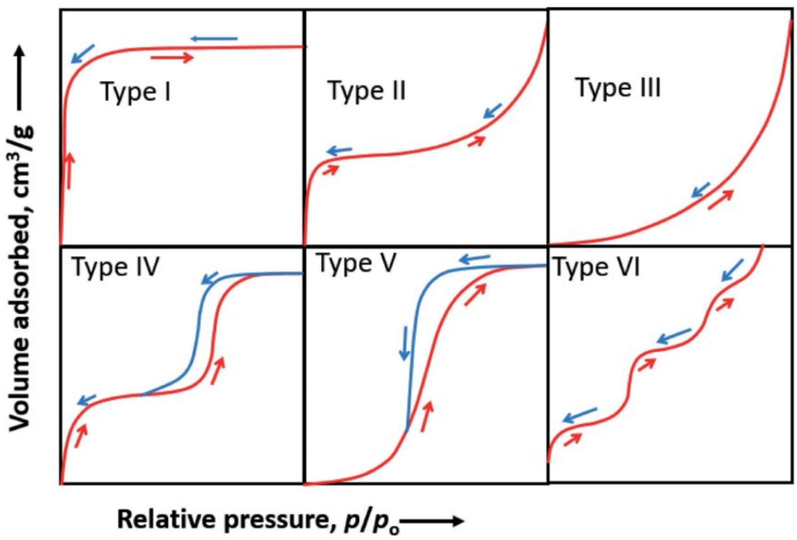

Figure 2. The six types of gas and vapour adsorption isotherms according to Brunauer (Kumar et al. 2019)

Type I follows the Langmuir's theory and has a monolayer of adsorption. These isotherms are met with solid adsorbents with micropores and quite small external surfaces. Type II is common with physisorption and relates to reversible multilayer adsorption with either macropore adsorbents or nonporous materials. Type III is not a common isotherm but can be found in for example the adsorption of bromine on silica gel. In this case the heat of adsorption is smaller or equal to the condensation heat of the pure adsorbate. There is no noticeable monolayer formation so the molecules form clusters around the accessible sites in microporous or nonporous adsorbents (Thommes et al. 2015). Types IV and V are corresponding to types II and III but the maximum adsorption is reached with a pressure lower than that of the saturated vapour p_0 (Ościk 1982). Type IV isotherm is met with mesoporous adsorbents and type V with adsorbents that have micropores or mesopores. Type VI isotherm has lower partial pressures of adsorbent-adsorbate interactions (Kumar et al. 2019) and gets its shape from the layer-by-layer adsorption. The adsorbents that give isotherm type VI are very uniform and nonporous (Thommes et al. 2015).

The common drawback of the theory's presented above is the neglection of horizontal interactions between the surface layer and adsorbate molecules. These horizontal interactions can be significant in for example adsorption of non-polar surface, of large molecules or when the adsorbate form hydrogen bonds with the adsorbent surface. These interactions result in the isotherm to bend towards the pressure axis (Ościk 1982).

4.1.2 Effect of sorbent pore structure on adsorption-desorption isotherms

In capillary condensation the pressure p is smaller than the saturation pressure p_0 and the gas condenses to liquid-like state within the pore. As the capillaries become narrow in the adsorbent, the adsorption forces that are applied by the walls can strengthen and the overall adsorption energy grow. The formation of capillary condensation hysteresis loop is caused by the formation of menisci in the pores that only burst when the gas pressure over a spherical liquid meniscus decreases lower than the surrounding pressure over a cylindrical liquid meniscus. The shape of the hysteresis loop depends on the shape of the pores (Ościk 1982). The different types of hysteresis loops are presented in Figure 3.

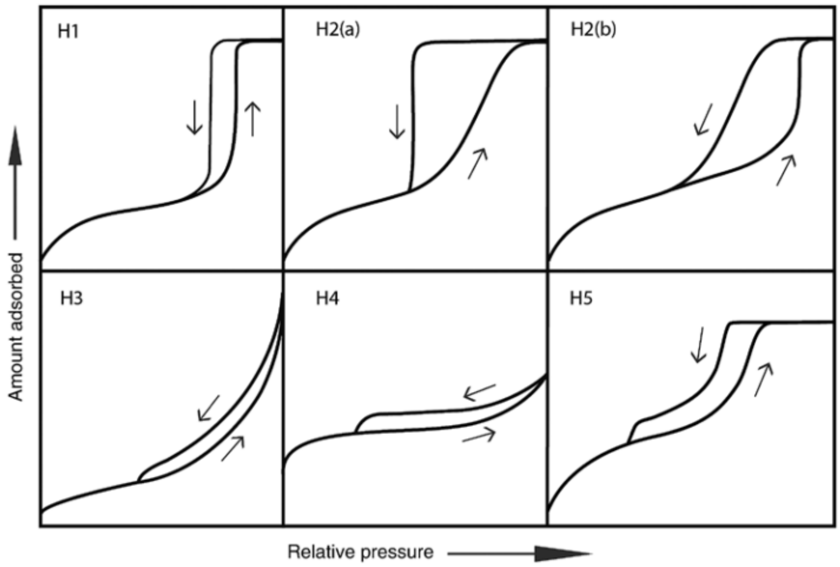

Figure 3. The types of hysteresis loops (Thommes et al. 2015)

Type H1 hysteresis is acquired if the capillaries are of narrow range and uniform. It can also occur in adsorbents with networks of ink-bottle pores. H2 type is obtained when the pores are more complex. In H2(a) the steep desorption branch is caused by pore-blocking or percolation in the narrow pore necks or evaporation caused by cavitation. H2(b) loops are found with materials that have larger pore size distribution than with H2(a) loop. With H3 the adsorption branch corresponds to type II isotherm and the minimum limit of desorption branch is placed at the cavitation-induced p/p_0. This can occur when the network has macropores (pores >50 nm) that are not entirely filled with the pore condense. H4 has adsorption branch that resembles type I. H5 is not as common but is obtained when the pores are both open and partially blocked mesopores (pores 2 nm – 50 nm) (Thommes et al. 2015).

4.2 Metal-organic frameworks (MOFs)

MOFs have attracted extensive interest among researchers for adsorption as they are a new emerging class of porous materials. MOFs are crystalline materials with extensive porosity that can reach up to 90% of free volume and ultrahigh internal surface areas (over 6 000 m^2/g). There is a vast variability for the organic and inorganic components in the structure. In addition, the pore sizes are tuneable and internal surface properties adjustable (Zhou et al. 2012).

MOFs show potential in applications in storage media for gases and high-capacity adsorbents as well as in membranes, clean energy, catalysis, and thin film devices (Zhou et al. 2012). Adsorption with MOFs can derive to superior adsorption capacities as well as selectivity for SO_2 and NO_X while keeping the structural integrity. Great structural stability and reusability are necessary for potential applications in removing SO_2 and NO_X (Han et al. 2019).

Empty spaces and voids in the lattice are generated by the directionality of the metal-ligand coordination bond. The strength of these coordinated forces determines the stability of the MOFs structure since those are typically the weakest links in the MOF. The activate sites in MOFs involve metal nodes, functional linkers, or the guests that are accommodated in the said voids. Structural defects can also work as active sites in catalysis (Gascon et al. 2014).

Separating two or more components with MOFs requires a differentiation in how the analyte gases interacts with the adsorbent. This can be executed by size or energetically. Energetically the adsorption can occur in two primary ways; by chemisorption where chemical transformation is responsible for the uptake of the gas or physisorption where the electric field from the framework and the guest molecule interact. Size exclusion selectivity require fine-tuning of the pore size which is usually very challenging (Hendon et al. 2017).

Incorporating open metal sites in the metal oxide cluster shows potential to designing an optimal surface chemistry for polar gas removal and providing a strong electrostatic or Lewis acid-Lewis base interaction for the electron-rich gases and electron-deficient open metal sites. Optimal metal type needs to be found for a specific gas that exhibits the strongest interaction (Kim 2018).

For non-polar gases the optimal strategy for gas adsorption would be to tune the surface chemistry by incorporating appropriate functionality. The surface chemistry needs to be optimized for all the individual gases separately (Kim 2018). The effect of dipole moment and polarizability for the adsorption is presented in Figure 4.

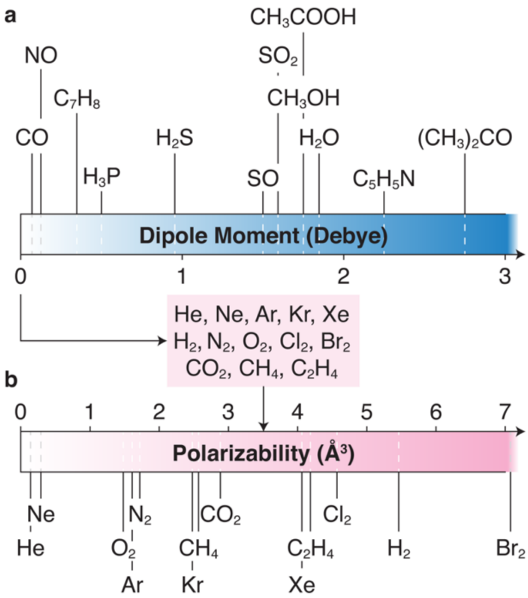

Figure 4. The effect of dipole moment and polarizability of the guest molecule (Hendon et al. 2017)

As seen from Figure 4, the interaction energy is closely linked to the magnitude of the dipole moment of the guest molecule. The higher the dipole moment, the higher the interaction energy and thus the adsorption capacity. For gases without a permanent dipole moment, polarization is the main factor affecting the selectivity. It is challenging to separate two compounds with comparable polarizabilities such as N_2 and O_2 (Hendon et al. 2017).

The overlap of the potential increases while pore size or volume decreases which leads to stronger enthalpic interactions with the adsorbent and adsorbate as well as the highest levels of adsorption. At high pressures however, the larger surface area and free volume result in more room for the guest molecules thus resulting in high uptakes (Son et al. 2014).

The common drawbacks in MOFs compared to inorganic porous solids include low thermal and chemical stability and the possible sensitivity to moisture (Gascon et al. 2014). Since the low stability of the MOFs is one of the main drawbacks considering the most fitting material for any application is needed. Especially the corrosive toxic gases can compromise the stability of the MOF used as adsorbent. NO_2 and SO_2 can affect the coordination bonds between the metal centres and organic ligands causing a breakdown in the MOF structure. (Martinez-Ahumada et al. 2021) In particular MOFs with Zr(IV), Al(III) and Mg(II) metal sites have shown great chemical stability (Jurado-Vázquez et al. 2018). Thermal stability is one of the key factors whether the MOF is suitable for a certain application and the thermal behaviour is crucial to know (Healy et al. 2020).

The common characteristics between the stable MOFs in the presence of corrosive gases are the force of the ligand-metal bond, the formation of supramolecular host-guest interactions, oxidation state of the metal centre and the robustness of the metal cluster. (Martinez-Ahumada et al. 2021) Open metal sites increase the adsorption of toxic gases in order of NH_3 > NO_2 > H_2S > NO > CO > SO_2. This means that for the adsorption of NO_2 the open metal sites make greater difference than for SO_2 (Daglar et al. 2022).

Further research is also needed in studies with conditions closer to realistic industrial applications (Martinez-Ahumada et al. 2021). Generally toxic gases are generated under wet conditions which leads to H_2O content in the gas mixture. H_2O molecules can cause low adsorption selectivity as they compete with the toxic gases for the adsorption sites and lead to decrease in crystallinity of the framework. This can potentially be avoided by with hydrophobic MOFs (Liu et al. 2015). In addition, only a few MOFs could be synthetized in an industrial scale as of now (Martinez-Ahumada et al. 2021). The common drawback regarding MOFs is their long-term stability. NO_2 and SO_2 are both corrosive gases that poses additional challenge to the stability of the adsorbent (Carter et al. 2020).

4.3 Adsorption of SO_2 with MOFs

MOFs with bigger than 0.4 nm pore sizes have the highest SO_2 gas adsorption capacities. Universally the quantity adsorbed correlates with the temperature of adsorption at low pressures. At moderate pressures the adsorption uptake is not well-correlated with the accessibility of surface area and free volume but they still play an important role in SO_2 adsorption and storage (Song et al. 2014).

The chemical nature of SO_2 can be exploited for MOF adsorption. The oxygen in SO_2 can act as a Lewis-base due to its richness in electrons and sulphur can be a Lewis acid site. The MOFs employed in SO_2 adsorption can be divided in four categories: open metal sites, μ-OH groups, defective sites, and halogen functionalisation (Martinez-Ahumada et al. 2021).

MOFs with defective sites include materials with crystal irregularities such as defects or inhomogeneities in composition. MOFs with defective sites offer very particular chemical and physical properties that are typically utilized in catalysis performances and filtering. Defective sites could also improve the adsorption capacities for SO_2 removal (Xiang et al.

2020). Several different MOFs with coordinatively unsaturated metal sites have been tested for SO_2 adsorption. The main difficulty with such MOFs is to find chemically stable options.

4.3.1 MOF-177

In a study made by Brandt et al. (2019) MOF-177 with open Zn^{2+} sites were tested for SO_2 separation. While the capture capacity shows great potential (25.7 mmol/g at 298 K and 1 bar) the chemical stability is a problem. The structure degraded partially after the exposure to SO_2 (Brandt et al. 2019).

4.3.2 MFM-170

Smith et al. used MFM-170 with open Cu^{2+} sites to adsorb SO_2 and found it to be highly stable in dry and moist conditions with adsorption capacity of 17.5 mmol/g at 298 K and 1 bar. This suggests that Cu^{2+} site is the strongest when it comes to thermodynamics to bind SO_2 while still being able to almost entirely desorb when reducing pressure. The selectivity of SO_2 over CO_2 is 35 and for SO_2/N_2 it is 944. The crystallinity is not compromised even by heating for the regeneration even after 50 adsorption-desorption cycles. This stability can be explained by the extraordinary paddlewheel SBU that is shaped in the framework and additional intermolecular interactions that are shaped between the pore walls of the framework and SO_2 (Smith et al. 2019).

4.3.3 MIL-101(Cr)

Martinez-Ahumad et al. (2020) studied partly fluorinated version of MIL-101(Cr) called MIL-101(Cr)-4F(1%). In this MOF the acidity of some of the Cr^{3+} centres is increased since fluorine attracts electrons. The adsorption capacity achieved was 18.4 mmol/g at 298 K and 1 bar. Chemical stability is great in dry and humid conditions and cycling performance exceptional. The SO_2 uptake occurs in three stages with MIL-101(Cr)-4F(1%). Firstly, there is adsorption at the acid (Lewis) sites of Cr^{3+} then there’s adsorption at Lewis and Brønsted acid sites, and lastly within the cavities of the MOF structure (Martinez-Ahumad et al. 2020).

4.3.4 MIL-160

In a study exhibited by Brandt et al. (2019) MIL-160 showed a lot of potential for SO_2 adsorption. The material exhibits outstanding performances in selectivity, breakthrough time and stability. It can also be regenerated in low temperatures (293 K). Even in low pressures the SO_2 uptake is high and with 0.97 bar capacity of 7.2 mmol/g is reached (Brandt et al. 209). The extremely high SO_2 uptake of MIL-160 may be caused by the material's structural flexibility. It is sensitive to SO_2 even at very low pressures (<0.001 bar) (Liu et al. 2021).

4.3.5 Cu-BTC

Cu-BTC (copper benzene-1,3,5-tricarboxylate) is composed of four benzene tricarboxylate groups that are coordinated to Cu(II) ions. (Wang et al. 2020) It is not chemically stable, and the decomposition temperature is quite low, 250–300ºC (Healy et al. 2020).

In a study executed by Sun et al. Cu-BTC and MIL-47 were stated the best out of twelve materials in terms of absolute adsorption, adsorption selectivity, working capacity for SO_2 adsorption. These materials include six different MOFs, two zeolitic imidazolate frameworks (ZIFs), and four zeolites; LTA, FAU, DDR, MFI, IRMOF-1, Cu-BTC, MIL-47(V), MOF-177, Mg-MOF-74, Zn-MOF-74, ZIF-8, and ZIF-10. Real post combustion flue gas is mimicked with a gas mixture containing 0.7975 N_2, 0.15 CO_2, 0.05 O_2, 0.002 SO_2, 250 ppm NO_2 and 250 ppm NO in volume fractions. The pressure was 1 bar and water vapour presence was neglected (Sun et al. 2014).

The materials were tested for absolute adsorption, working capacity and adsorption selectivity. The best absolute adsorption of SO_2 was received with Mg-MOF-74, MIL-47 and Cu-BTC. Mg-MOF-74, MIL-47 and Cu-BTC also had the best execution of working capacity for SO_2, NO_X and CO_2. For selectivity the best performance was achieved with MIL-47, MFI and Cu-BTC. Mg-MOF-74 was not included in the top materials regarding selectivity due to its large uptake of CO_2. This is because Mg-MOF-74 has the topmost density of open-metal sites compared to the other materials. Its larger quadrupole moment in addition to higher polarizability of CO_2 favours the adsorption in the open-metal sites. Also, the composition of CO_2 is the second greatest in the flue gas mixture. This is why CO_2

will be more likely to be adsorbed in Mg-MOF-74 compared to other guest molecules in the gas mixture (Sun et al. 2014).

The study executed by Wang et al. (2020) showed the preferential adsorption of SO_2 compared to CO_2 using Cu-BTC. The selectivity for SO_2 is high in CO_2/SO_2 mixture. The high SO_2 selectivity can be explained by the unique structure with three domain types. There are tetrahedron side pockets, cuboctahedral cages and large square shaped channels. The uptake of SO_2 molecules decrease as the temperature gets higher (Wang et al. 2020). However, the adsorption capacity is only 0.499 mmol/g which is comparable to that of generally used granular activates carbon, so the use of MOF gives no advantage (Han et al. 2019).

4.3.6 Mg-MOF-74

MOF-74 contains infinite chain-like secondary building units that are connected to a honeycomb arrangement with bridging 2,5-dioxidoterephthalate linkers. The decomposition temperature is approximately 350 ºC (Healy et al. 2020).

It is known that Mg-MOF-74 is not structurally stable in water. Since MOFs can form one coordinatively unsaturated site per one metal centre, they can adsorb one gas molecule per metal centre. In the case of SO_X and H_2O the preferred binding is for SO_X over the water molecules. In the study executed by Henkelis et al. Mg-MOF-74 with humid SOX gas mixture showed full structural integrity and crystallinity before the maximum available adsorption was reached. After that, in this study after the third day partial structural collapse took place. It was also seen that the MOF was not able to have the SOX forcefully removed without some structural collapse (Henkelis et al. 2021).

SO_2 is only molecularly adsorbed into MOF-74 and binds strongly to Mg-MOF-74 due to its high binding energy. For Mg-MOF-74 the binding energy is approximately 90 kJ/mol and for Zn-MOF-74 it's about 70 kJ/mol. SO_2 uptake of 8.60 mmol/g was achieved in 1.02 bar with Mg-MOF-74 (Tan et al. 2017).

4.3.7 MFM-300

MOFs containing μ-OH groups include for example MFM-300. The MOF-300(M) (M = Al^{3+}, In^{3+}, Ga^{3+} and Sc^{3+}) family presents results with high chemical stability towards SO_2. The most potential adsorption in the MFM-300 family was executed with MFM-300(Sc) with adsorption capacity of 9.4 mmol/g with chemical stability in dry and moist conditions over 10 cycles. The reason for MFM-300 materials high chemical stability and remarkable cyclability and facile regeneration is the strength of the bonds between the oxygen atoms and the metal centres (Savage et al. 2016). SO_2 uptake increases whit low pressures (below 50 mbar) which can be explained by the high dipole moment of SO_2. The selectivity of SO_2 over CO_2 is higher with low pressures (1 bar and 273 K) with fillings of 69% and 82% of the pore volume respectively (Yang et al.2012).

As the active hydroxyl groups in the pore channels in MFM-300(Al) interact with SO_2 the formation of Al-OH···O=S=O hydrogen bonds occurs. This is supplemented with weaker phenyl C-H···O=S=O contacts surrounding the pore (Yang et al. 2012).

MFM-300(In) exhibits a very high SO_2 uptake of 8.28 mmol/g at 298 K and 1 bar with SO_2/CO_2 selectivity of 60 and SO_2/N_2 selectivity of 5000 at 298 K and 1 bar. It also has a very high stability showing a lot of potential for SO_2 adsorption (Savage et al. 2016). At low pressures (<0.01 bar) SO_2 uptake is very weak but has a higher uptake compared to MIL-160 in higher pressures. The pore size of the material is approximately 6.5 Å which explains the high uptake. The uptake decreases slightly in the presence of H_2O. With a H_2O molar fraction over 0.5 % the decrease in the uptake is significant. Since flue gas usually contain 5-7% water, dehydration is required (Liu et al. 2021).

4.3.8 SIFSIX-1-Cu

The last group of MOFs are materials with halogen functionalisation. When halogen counterions are present in a porous material, SO_2 capture performance enhances because of the involvement of ionic bonding (Suo et al. 2021). This group includes SIFSIX materials.

Cui and co-workers studied the adsorption of SO_2 with anion-pillared hybrid porous materials. Extraordinary adsorption capacity of 11.01 mmol/g was achieved even in trace amounts of SO_2 with SIFSIX-1-Cu. The selectivity of SO_2/CO_2 is in the range 86–89 (Cui et al. 2017).

SO_2 adsorption capacities of different MOFs are presented in Table 4.

Table 4. SO_2 adsorption capacities of different MOFs in 298 K and 1 bar

MOF	BET surface area, (m^2/g)	Pore volume, (cm^3/g)	Adsorption capacity, (mmol/g)	SO_2/ CO_2	SO_2/ N_2	Regenaration temperature, (ºC)	Reference
MOF-177[1]	[c]3875	[b]1.59	[a]25.7				[a](Brandt et al. 2017) [b](Li & Yang 2007)
MFM-170	2408	0.88	17.5	35	944	25	(Smith et al. 2019)
MOF-74(Mg)	[d]1206	[d]0.28	[c]8.6			[e]120	[c](Tan et al. 2017), [d](Zhang et al. 2022) [e](Glover et al. 2011)
MIL-101(Cr)-4F(1%)	[g]2916	[g]2.02	[f]18.4			[f]25	[f](Martinez-Ahumad et al. 2020), [g](Yu et al. 2017)
MIL-160[2]	[h]1120	[i]0.46	[h]7.2	[h]124-128	[i]31.25	[i]20	[h](Brandt et al. 2019), [i](Permyakova et al. 2017)
MFM-300(Sc)	1350	~0.4	9.4			25	(Savage et al. 2016)
MFM-300(Al)[3]	1370	~0.4	8.1	53	6 522	25	(Yang et al. 2012)

MFM-300(In)	1071	0.419	8.28	60	5 000	25	(Martinez-Ahumada et a. 2021)
SIFSIX-1-Cu			11.0	70.7	3 145.7	40	(Cui et al. 2017)
Cu-BTC	[j]909	[j]0.471	[j]0.499			[k]140	[j](Han et al. 2019) [k](Wang et al. 2020)

[1]295 K, 1 bar
[2]298 K, 0.97 bar
[3]273 K, 1 bar

In conclusion the most promising materials for SO_2 adsorption are MIL-1010(Cr)-4F(1%), MFM-170, SIFSIX-1-Cu, MFM-300 and MIL-160. All these materials show great chemical stability, selectivity, and adsorption capacity.

4.4 Adsorption of NO_2 with MOFs

Several studies show drawbacks in NO_X removal with MOFs due to the decomposition of MOFs to some extent during the adsorption, so it is required to find a MOF that is chemically stable and performs a reversible adsorption (Han et al. 2019).

4.4.1 UiO-66 (UiO = University of Oslo)

UiO-66 consists of connected $[Zr_6O_4(OH)_4]_{12}+$ nodes that are linked together by benzene-1,4-dicarboxylate ligands. The material contains both tetrahedral and octahedral voids in the framework. Decomposition temperature of UiO-66 is approximately 425–500 ºC. As the material decomposes benzene and CO_2 are released resulting in formation of zirconia (Healy et al. 2020).

Organic linkers have a key role in the capture of NO_2. UiO-66 and Ui-O-NH_2 have been studied for NO_2 removal by Peterson et al. (2016). Experiments were executed in dry and humid conditions. In dry conditions UiO-66-NH_2 has the adsorption capacity of 20.3 mmol/g and UiO-66 8.8 mmol/g. In humid conditions the adsorption capacities were 31.2 mmol/g and 20.3 mmol/g respectively. UiO-66-NH_2 also produces noticeably less NO as a side product compared to UiO-66. These differences are explained by the superior capability of H_2O adsorption of UiO-66-NH_2. H_2O adsorption in the pore network enhances increases the stabilization of NO_2 molecules due to the development of supramolecular interactions. It enables the desired formation of nitrous acid as a by-product (Peterson et al. 2016).

The crystallinity of UiO-66-NH2 is stable and remains undamaged but the reactivity of the adsorbate results to a reaction chain with the organic linker which then ends up in the post functionalization of the phenyl group (Peterson et al. 2016).

4.4.2 Cu-BTC

NO_2 uptake of 2.3 mmol/g in dry conditions and 1.17 mmol/g in wet conditions was achieved in a study exhibited by Levasseur et al. (2010). In addition to the relatively low adsorption capacity the partial destruction of the porosity makes the material insignificant in relates to NO_2 abduction (Levasseur et al. 2010).

For the removal of NO_X from the flue gas Cu-BTC has great absolute absorption, selectivity and working capacity. However, it's performance in the removal of NO_X is much lower than in SO_2 (Sun et al. 2014).

4.4.3 MFM-300(Al)

In a study implemented by Han et al. (2018) MFM-300(Al) was used for NO_2 removal. The reactive NO_2 are stabilised in the pore network by the synergistic effect between the inorganic building block and the organic ligand in MFM-300(Al). A fully reversible NO_2 uptake of 14.1 mmol/g was achieved with the MOF at 298 K and 1 bar. Chemical stability remains intact after five cycles. This adsorption material shows great potential for a selective NO_X removal (from 5 000 ppm to < 1 ppm) and both in dry and humid conditions. The outstanding performance can be explained by the existence of the host-guest and guest-guest interactions. Host-guest interactions involves principally the hydrogen bonding between NOx and -OH pendant group from the inorganic node. Guest-guest interactions refers to the guest molecules in their monomeric (NO_2) and dimeric (N_2O_4) forms and the supramolecular interactions between them confined within the pore network (Han et al. 2018).

In humid conditions the breakthrough and breakthrough time of NO_2 from MFM-300(Al) is slightly reduced due to the competitive adsorption of water. Stability of the MOF is remained. The selectivity of NO_2 with MFM-300(Al) is higher compared to CO_2 or SO_2. Approximately 7.73 g/cm^3 density of adsorbed NO_2 molecules in MFM-300(Al) is achieved. That is higher than the densities of liquid NO_2 (1.45 g/cm^3) or liquid N_2O_4 (1.44 g/cm^3) but lower than the density of solid N_2O_4 (1.94 g/cm^3 at 140 K) (Han et al. 2018).

4.4.4 Mg-MOF-74

When NO_2 is adsorbed with M-MOF-74 (M=Mg, Zn, Ni, Co) it dissociatively adsorbs into the compound and forms nitrate species and NO through decomposition or disproportionation reactions. This can be explained by the transfer of charge from the N-O bond to the MOF which weakens the bond of nitric oxide but enables the dissociation reaction. (Tan et al. 2017) This follows the reaction pathways in reactions r_{12} and r_{13} (Rodriguez & Jirsak 2000).

$$NO_2(ads) + M - O \xrightarrow{r_{12}} Mg - NO_3(ads) \tag{12}$$

$$2NO_2(ads) \xrightarrow{r_{13}} NO_3^-(ads) + NO(gas) \tag{13}$$

The potential MOFs for NO_2 adsorption are presented and compared in Table 5. In conclusion the only MOF for NO_2 adsorption with very high adsorption capacity, selectivity and chemical stability is MFM-300(Al).

Table 5. MOFs for adsorption of NO_2

MOF	BET surface area (m^2/g)	Pore volume, (cm^3/g)	Adsorption capacity, (mmol/g)	NO_2/CO_2	NO_2/N_2	Regenaration temperature, (ºC)	References
UiO-66-NH_2[1]	987	0.4	31.2				(Peterson et al. 2016)
MFM-300(Al)[2]	1.37	~0.4	14.1	248	$>10^4$		(Han et al. 2018)
Cu-BTC[3]	909	0.471	2.3 (dry) 1.17 (wet)				(Levasseur et al. 2010)
Mg-MOF-74[4]	[a]1206	[b]0.28	[c]1.4				[a](Tan et al. 2017), [b](Zhang et al. 2022) [c](Sun et al. 2014)

[1]500-700 ppm NO_2/air, 293 K
[2] Pure NO_2, 295 K, 1 bar
[3]1000 ppm NO_2/air, 298 K
[4]298 K, 1 bar

4.5 Simultaneous adsorption of SO_2 and NO_2 with MOFs

For the simultaneous removal of SO_2, NO_X and CO_2, Mg-MOF-47 was studied by Sun et al (2014) with a gas mixture with volume fractions of 0.7975 N_2, 0.15 CO_2, 0.05 O_2, 0.002 SO_2, 250 ppm NO_2 and 250 ppm NO. The uptake of CO_2 is the biggest of the three, but so is CO_2 content in the flue gas mixture compared to SO_2 and NO_X. That is due to the preferential binding of CO_2 over SO_2 and NO_2 (Sun et al. 2014).

In conclusion the study made by Sun et al. shows that Cu-BTC is the most promising material out of the ones considered for removing SO_2 and NO_X separately although due to the small dipole moment of NO_X all the materials including Cu-BTC are not able to provide a separation with great capacity and high selectivity. For the simultaneous removal of SO_2, NO_X and CO_2 the only promising adsorption material of the studied MOFs is Mg-MOF-74. This can be explained by the high density of open-metal sites which supply strong interactions with quadruple and dipole molecules (Sun et al. 2014).

In a study executed by (Glover et al. 2011) MOF-74 with different metal centres were tested for ammonia, cyanogen chloride and sulphur dioxide adsorption in dry and humid conditions. The unsaturated metal sites can be varied while not affecting the underlying framework structure (Glover et al. 2011).

The gas mixture used in the study contained acid adsorbates, cyanogen chloride, sulphur dioxide, ammonia, and octane. Between these variations the Mg-MOF-74 shows the best results. It can be seen from the results that the humidity of the gas mixture affects the adsorption capacity negatively. For example, sulphur dioxide loading in dry conditions is 1.6 mol/kg and in wet conditions 0.72 mol/kg with Mg-MOF-74 (Glover et al. 2011).

All the previously presented MOFs that can separate both SO_2 and NO_2 are collected in Table 6. The drawbacks of Mg-MOF-74 are the chemical instability in humid conditions and poor selectivity for NO_2. Cu-BTC is not stable once it's in connection with SO_2 and NO_2 and the uptake is not high enough. This leaves the MFM-300(Al) the only reasonable option with great adsorption capacity, high chemical and thermal stabilities and great selectivity for SO_2 and NO_2.

Table 6. List of MOFs that can be used for SO_2 and NO_2 reduction and their stability and adsorption capacity

MOF	SO_2 adsorption capacity, (mmol/g)	NO_2 adsorption capacity, (mmol/g)	SO2 regenaration temperature, (ºC)	NO2 regenaration temperature, (ºC)	Decomposition temperature, (ºC)	Reference
Mg-MOF-74	[1]8.6	[2]1.4	[3]120		[1]300	[1](Tan et al. 2017) [2](Sun et al. 2014) [3](Glover et al. 2011)
MFM-300(Al)	[4]7.1	[4]14.1	[5]25		[6]400	[4](Savage et al. 2016), [6](Han et al. 2018) [5](Yang et al. 2012)
Cu-BTC	[6]0.499	[6]1.17–2.3	[7]140		[6]250–300	[6](Sun et al. 2014) [7](Wang et al. 2020)

4.6 MFM-300(Al)

Since MFM-300(Al) (also called NOTT-300) is the only promising MOF for both SO_2 and NO_2 adsorption found in the literature that is stable in humid conditions, it is chosen for the laboratory tests. The adsorption capacity and selectivity are promising for both SO_2 and NO_2.

The MFM-300(M) family (M=Sc, Al, In, Ga_2, Fe_2, V^{III}, Fe) is known for the high thermal stability, stability at wide pH range (1-11) and water stability. (Jurado-Vázquez et al. 2019) The general chemical equation of the MFM-300 group is $[M_2(OH)_2(L)]$(H_4L=biphenyl-

3,3’,5,’5-tetra-carboxylic acid=$C_{16}O_8H_6$). MFM-300 are highly porous with one-dimensional pore channels arranged in a ‘wine rack’ display (Savage et al. 2016).

Within the MFM-300(M) series the aluminium MFM-300 is particularly stable (Carter et al. 2020). Aluminium is also more accessible and affordable compared to other metals (Liu et al. 2021). The material shows especially high adsorption selectivity for CO_2 and SO_2. While in a study executed by Yang et al. (2012) the adsorption of SO_2 and CO_2 reached 8.0 mmol/g and 6.1 mmol/g the adsorptions of CH_4, CO, N_2, H_2, O_2 and Ar only showed surface adsorption behaviours with low uptakes of 0.04-0.25 mmol/g (Yang et al. 2012). Different selectivity values are presented in Table 7.

Table 7. Selectivity for SO_2 and NO_2 over other components with MFM-300(Al) in 298 K and 1 bar (Yang et al. 2012), (Han et al. 2018)

Components	Selectivity (mol/mol)
SO_2/CH_4	3 620
SO_2/N_2	6 522
SO_2/H_2	$>10^5$
SO_2/CO_2	53
NO_2/SO_2	18.1
NO_2/CO_2	248
NO_2/N_2	$>10^4$

The structure of MFM-300(Al) contains chains of $[AlO_4(OH)_2]$ that are bridged by tetracarboxylate ligands L^{4-}. Al(III) ion bounds to six oxygen donors that are from carboxylates and bridging hydroxyl group μ_2-OH. The *cis*-μ_2-OH groups offer chirality and rigidity for the framework in MFM-300(Al). This also forms the square-shaped channels in the material. The approximate diameter of the channel window is 6.5 × 6.5 Å (Yang et al. 2012). The structures of the octahedral chain and the framework are presented in Figure 5 and Figure 6.

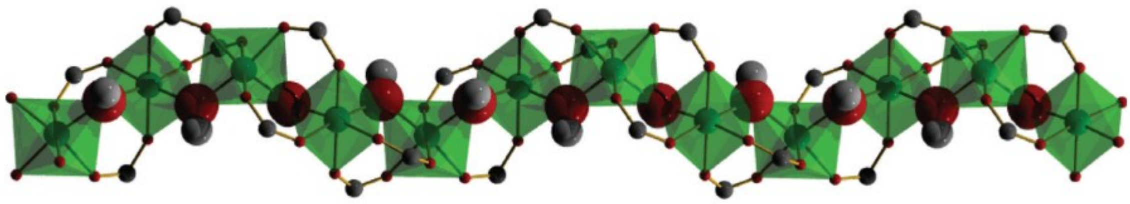

Figure 5. The structure of the octahedral chain of $[AlO_4(OH)_2]_\infty$ (Yang et al. 2012)

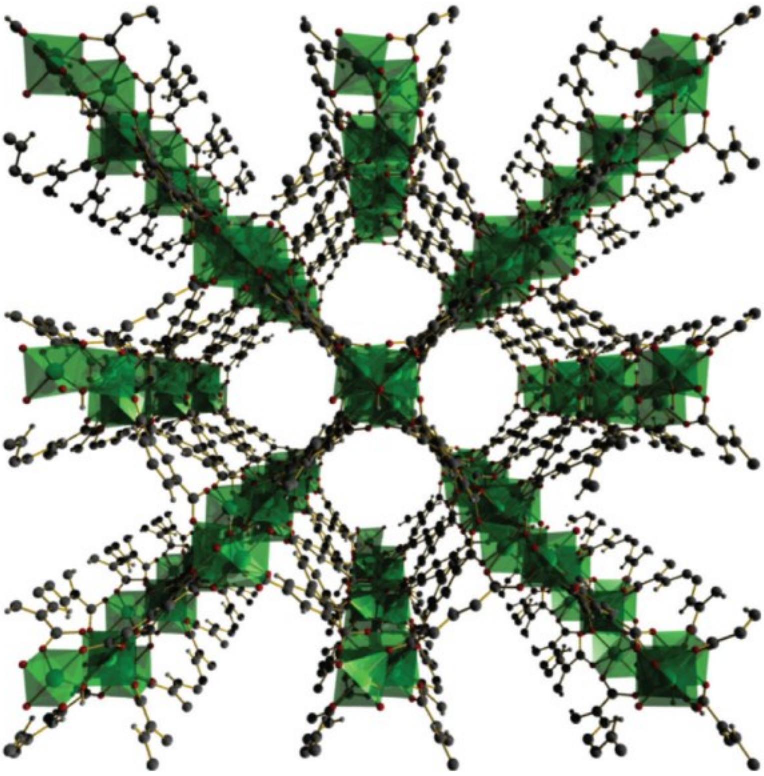

Figure 6. The three-dimensional framework structure of MFM-300(Al). Aluminium is marked green, carbon grey, oxygen red and hydrogen white, $[AlO_4(OH)_2]$ is the green octahedron (Yang et al. 2012)

The thermal stability of MFM-300(Al) reaches up to 400 ºC. It is also stabile towards humidity air, and the general organic solvents. It can be rehydrated with retention. Even after multiple hydration-dehydration cycles the framework porosity and surface area remain untouched. Full reversibility can be achieved without hysteresis and regeneration can be done in ambient temperatures which eliminates the energy requirement of heating (Yang et al. 2012).

The study conducted by Carter et al. (2020) shows that even long-term stability is achieved with MFM-300(Al) and corrosive gases of NO_2 and SO_2. Storing capability of 120 is achieved for NO_2. Long term stability for SO_2 is weaker but this poses no issues due to the need for short time retainment of SO_2 for safe transport (Carter et al. 2020). Physical characteristics of MFM-300(Al) are presented in Table 8.

Table 8. Physical characteristics of MFM-300(Al) (Wu et al. 2018)

Parameter (unit)	Values
Dimensions (Å^3)	20 755.35
Bulk density (g/cm$^{3)}$	1.06
Surface area (m^2/g)	1 340.69
Available pore volume V_p^c (cm^3/g)	0.44
Porosity ϕ_c (%)	46.67

Compared to other members of the MFM-300(M) family, the MFM-300(Al) has the smallest porosity. Porosity ranges from 46.67% to 51.74% and follows the sequence MFM-300(In) > MFM-300(Ga) > MFM-300(Al) (Wu et al. 2018).

5 Modelling of adsorption

The adsorption of NO_2, SO_2 and N_2 are modelled with MFM-300(Al) as the adsorbent. The modelling is done by CFD (computational fluid dynamics) modelling and using COMSOL Multiphysics 6.0 software.

5.1 Equilibrium isotherms

According to the Langmuir's theory of adsorption there is a certain number of active sites on adsorbent surface and at each only one molecule can be adsorbed. The bonding needs to be strong enough to not displace the adsorbed molecules along the surface, but it may be chemical or physical. When Langmuir's theory is employed for separating component i from a gas mixture the adsorption isotherm follows Eq. (14).

$$qi = \frac{q_m b p_i}{1 + b p_i} \tag{14}$$

Where, q_m is the maximum adsorption capacity at any p_i; b is the adsorption affinity; p_i is the partial pressure of the mixture components.

According to Eq. (14) the adsorption of the component i of a multicomponent gas mixture increases as its the partial pressure increases and the partial pressure of the other components decrease. Langmuir's theory is based on the adsorbent only forming monolayers so multilayer adsorption is ignored (Ościk 1982).

Another well-known adsorption isotherm is the Freundlich isotherm which follows Eq. (15).

$$q_i = k_{Fr} p_i^{\frac{1}{n_{Fr}}} \tag{15}$$

Where, k_{Fr} is the Freundlich model parameter; n_{Fr} is the Freundlich model exponential parameter.

Sips Model follows Eq. (16).

$$q_i = \frac{q_m (b p_i)^{\frac{1}{n_{Sips}}}}{1 + (b p_i)^{\frac{1}{n_{Sips}}}} \tag{16}$$

Where n_{Sips} is the Sips model exponential parameter.

The Toth isotherm equation has the form presented in Eq. (17).

$$q_i = \frac{q_m b p}{(1 + (bp)^t)^{\frac{1}{t}}} \tag{17}$$

Where t_{Toth} is the Toth model exponential parameter.

To demonstrate the adsorption uptake, adsorption isotherms are plotted. In y-axis the amount adsorbed is given in mol/g and on x-axis the equilibrium relative pressure p/p^0, in which the p^0 is the saturation pressure for the adsorbate (Thommes et al. 2015).

5.2 Governing equations

The mass transfer of the model is given by:

$$\frac{\partial(\epsilon_p C_{i)}}{\partial t} + \frac{\partial(\rho C_{p,i})}{\partial t} + \nabla \cdot J_i + u \cdot \nabla C_i = R_i + S_i \tag{18}$$

Where; ϵ_p is the bed porosity, t is the time (s), ρ is the density (kg/m^3), C_p is the specific heat capacity at constant stress (J/(kg K)), u is the velocity vector (m/s), S is particle specific surface area (m^2).

$$J_i = -(D_{D,i} + D_{e,i})\nabla c_i \tag{19}$$

Where; D is the thermal diffusion coefficient (kg/(m s))

Diffusion is given by:

$$D_{e,i} = \frac{\epsilon_p}{\tau_{F,i}} D_{F,i} \tag{20}$$

Where; $D_{e,i}$ is thermal diffusion coefficient (kg/(m s), D_F is the fluid diffusion coefficient of the component (m^2/s).

Millington and Quirk model is used for the effective diffusivity.

$$\tau_{F,i} = \epsilon_p^{-\frac{1}{3}} \tag{21}$$

Momentum equations of the model are given by:

$$\frac{\partial(\rho c_{p,i)}}{\partial t} = \rho K_{P,i} \frac{\partial c_i}{\partial t} - c_{P,i}\rho_s \frac{\partial \epsilon_p}{\partial t} = R_{ads,i} \tag{19}$$

$$K_{P,i} = \frac{\partial c_{P,i}}{\partial c_i} \tag{21}$$

$$\rho_s = \frac{\rho}{(1-\epsilon_p)} \tag{22}$$

Adsorption is given by the Langmuir model:

$$c_{P,i,L} = \frac{K_{L,i}c_{Pmax,i}c_i}{1 + K_{L,i}c_i} \quad (23)$$

Where; $K_{L,i}$ is the Langmuir constant (m^3/mol), $c_{P,max,i}$ is the adsorption maximum (mol/kg) and c is the concentration (mol/m^3).

Heat transfer in porous media follow Eq. (19) and Eq. (20).

$$d_z(\rho C_p)_{eff}\frac{\partial T}{\partial t} + d_z\rho_f c_{p,f}u \cdot \nabla T + \nabla \cdot q = d_z Q + q_0 + d_z Q_p + d_z Q_{vd} + d_z Q_{geo} \quad (19)$$

Where; d_z is the Out-of-Plane thickess (m), T is the absolute temperature (K), q is the heat flux by conduction (W/m^2), Q is heat source (W/m^3).

$$q = -d_x k_{eff}\nabla T \quad (20)$$

$$(\rho c_p)_{eff} = \epsilon_p \rho_f c_{p,f} + \theta_s \rho_s c_{p,s} + \theta_{imf}\theta_{imf}c_{p,imf} \quad (21)$$

Where; θ_s is the solid volume fraction, ϵ_p is the bed porosity.

$$k_{eff} = \epsilon_p k_f + \theta_s k_s + \theta_{imf}k_{imf} + k_{disp} \quad (22)$$

Where; k_f is the thermal conductivity (W/(m K))

$$k_s = \frac{k_b}{\theta_s} \quad (23)$$

Where; k_b is the dry bulk thermal conductivity (W/(m K)).

$$\rho_s = \frac{\rho_b}{\theta_s} \quad (24)$$

Where; ρ_b is the dry bulk density (kg/m^3).

$$c_{p,s} = \frac{C_{p,b}}{\theta_s} \quad (25)$$

Where; $C_{p,b}$ is the dry bulk heat capacity (J/(kg K))

5.3 Boundary and initial conditions

Initially the concentration of the adsorbed gases on the column is 0 mol/m3 and the temperature is 25 °C.

5.4 Physical model

The model is built according to the column on MixSorb SHP breakthrough analyser (3P Instruments, Germany). The column is presented as a 2D model that is a rectangle with 4.5 mm width and 65 mm long. Gas mixture goes through a column filled with adsorbent and the concentration adsorbed to MFM-300(Al) is detected. The flow goes through the column entering the column at the top and continuing towards the bottom. The geometry of the column is presented in Figure 7.

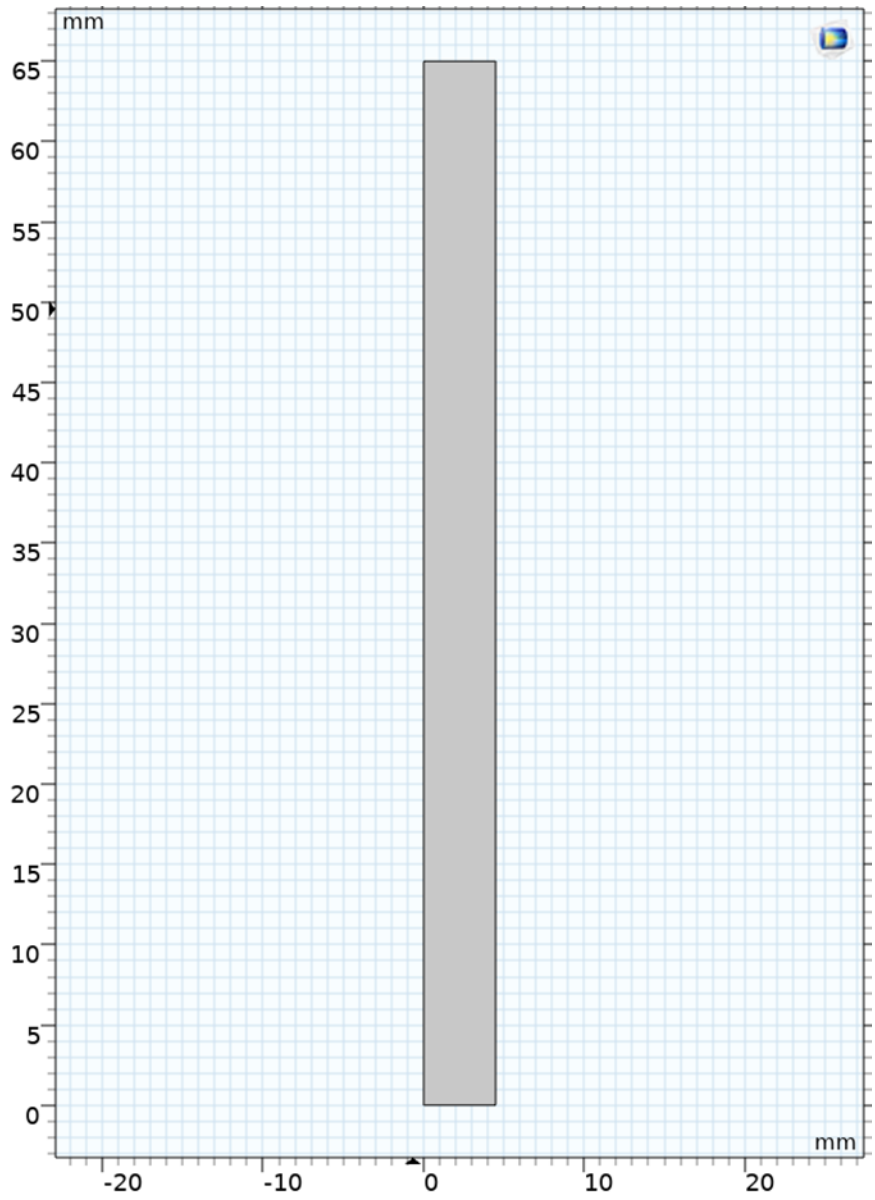

Figure 7. The geometry of the modelled column

5.5 Model assumptions

It is assumed that the MOF is packed homogeneously throughout the column and that there is no channelling. Radial concentration distribution is neglected. Experiment conditions are assumed to be isothermal and temperature change upon adsorption is neglected. For the heat transfer in porous media, the pressure work and viscous dissipation are neglected. It is assumed that thermal equilibrium holds, following similar temperature in the fluid and solid phase. Adsorption capacity is assumed to be similar through all the MOF. The powder in the column is assumed to be packed compactly and MOF porosity is used as bed porosity.

5.6 Numerical solution

The adsorption experiments are modelled using COMSOL Multiphysics 6.0. The simulations are made separately for three different cases: for a run with pure SO_2, for pure NO_2 and for both SO_2 and NO_2 with N_2. The model is built with the transport of diluted species in porous media and heat transfer in porous media physics interfaces and calculations are executed with the dynamic solver. Fine mesh size is used and the geometry of it is presented in Figure 8.

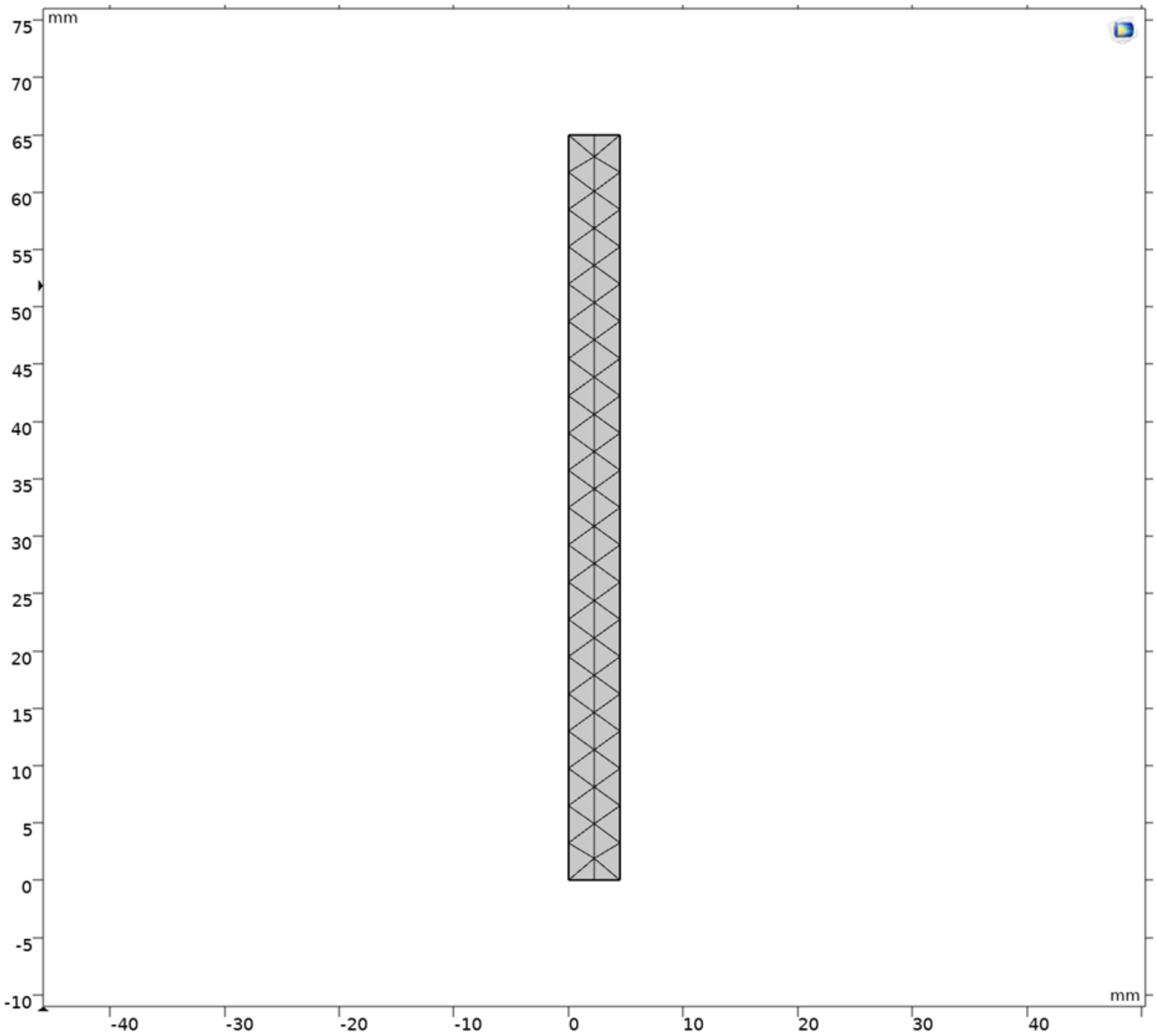

Figure 8. Fine mesh on the COMSOL model

Model parameters used for the simulation are presented in Tables (9-11).

Table 9. Model parameters for simulation I with SO_2

Parameter	Value (unit)	Remark
c01	0.9 (mol/m³)	Component 1 inlet concentration
rho_p	1 060 (kg/m³)	Density of solid particle
eps_p	0.4667	Porosity
v_l	0.1 (m/s)	Linear velocity, mobile phase
D_1	1 (cm²/s)	Diffusion coefficient, comp1
K1	38.64 (m³/mol)	Langmuir adsorption constant, component 1
n01	5.28 (mol/m²)	Monolayer capacity, comp1

Table 10. Model parameters for simulation II with NO2

Parameter	Value (unit)	Remark
c01	0.9 (mol/m³)	Component 1 inlet concentration
rho_p	1 060 (kg/m³)	Density of solid particle
eps_p	0.4667	Porosity
v_l	0.1 (m/s)	Linear velocity, mobile phase
D_1	1.08 (cm²/s)	Diffusion coefficient, comp1
K1	16.63 (m³/mol)	Langmuir adsorption constant, component 1
n01	15.41 (mol/m²)	Monolayer capacity, comp1

Table 11. Model parameters for simulation III with SO2, NO2 and N2

Parameter	Value (unit)	Remark
c01	0.9 (mol/m³)	NO_2 inlet concentration
c02	0.9 (mol/m³)	N_2 inlet concentration
c03	0.9 (mol/m³)	SO_2 inlet concentration
rho_p	1 060 (kg/m³)	Density of solid particle
eps_p	0.4667	Porosity
v_l	0.1 (m/s)	Linear velocity, mobile phase
D_1	1.08 (cm²/s)	Diffusion coefficient, NO_2
D_2	1 (cm²/s)	Diffusion coefficient, N_2
D_3	1 (cm2/s)	Diffusion coefficient, SO_2

K1	16.63 (m^3/mol)	Langmuir adsorption constant, NO_2
K2	3.275 (m^3/mol)	Langmuir adsorption constant, N_2
K3	38.64 (m^3/mol)	Langmuir adsorption constant, SO_2
n01	15.41 (mol/m^2)	Monolayer capacity, NO_2
n02	0.05155 (mol/m^2)	Monolayer capacity, N_2
n03	5.28 (mol/m^2)	Monolayer capacity, SO_2

6 Experimental methods

6.1 Materials used

For the synthetisation of the MOF two chemicals are used: biphenyl-3,3’,5,5’-tetracarboxylic acid (94%, Thermo scientific) and aluminium chloride-6-hydrate (99.5%, Riedel-de Haën).

6.2 Synthesizing the MOF

In microwave assisted synthesis, electromagnetic waves and mobile electric charges are employed. Because of the direct interaction between the radiation and the solution or reactant, microwave assisted synthesis is very energy efficient heating. This results in the possibility of high heating rates and very homogeneous heating throughout the sample. The benefits of microwave assisted synthesis is formation of nanoscale products, the rapid forming of crystallization, improvements in product purity and selective synthesis of polymorphs (Stock & Biswas 2012).

MFM-300(Al) is synthesized by hydrothermal reaction of H4BPTC (biphenyl-3,3’,5,5’-tetracarboxylic acid) and $AlCl_3 \cdot 6H_2O$. 250 mg of $AlCl_3 \cdot 6H_2O$ is mixed with 85 mg of H4BPTC and 15 mL of deionized water in 35 mL vial. The vial is then sealed and stirred. It is placed in microwave cavity (Discover 2.0, CEM), stirred, and heated to 210 °C with 300 W for 10 minutes in autogenous pressure. After the 10 minutes vial is let to cool in air. The suspension is centrifigated with 4 200 rpm and washed with distilled water. This step is repeated twice. The supernatant can be decanted, and the remnant powder dried in the oven at 50 °C for 18 hours. The sample is then kept at the fume hood and allowed to rehydrate (Thomas-Hillman et al. 2019).

This method of synthesizing can be viewed as a green synthesis since no organic solvents are used and toxic Pd(0) catalyst is not required. This accounts to cost effective, feasible and environmentally friendly process to scale up (Yang et al. 2012). This method produces higher quality material with significantly less time. In microwave synthesizer MFM-300(Al) can be produced in 10 minutes as opposed to the three-day conventional method (Thomas-Hillman et al. 2019).

6.3 Characterisation

The sample is characterized by scanning electron microscope (SEM), thermogravimetric analysis (TGA), BET analysis and x-ray diffraction (XRD). SEM analysis is conducted using the Hitachi SU3500 SEM equipment. BET analysis is executed with Micromeritics 3Flex BET analysis system and the pretreatment is done using Micromeritics Smart VacPrep. The equipment used for XRD is PANalytical Empyrean 3 diffractometer (Cu tube, $\lambda = 0.15406$ nm) equipped with poly-capillary optics (slit controlled beam size with height of 1 mm and width of 8 mm) and a PIXcel3D-Medipix3 detector.

6.3.1 SEM

Scanning electron microscope is used to study the particle sizes and shapes. EDS analysis is done with the SEM to study the weight % of each element in the SEM pictures.

6.3.2 Brunauer, Emmett and Teller (BET) adsorption theory

BET adsorption theory takes into consideration the multilayer vapor adsorption and it is based on the Langmuir theory assuming it to apply to every layer of adsorption. (Ościk 1982) The BET equation in its linear form is presented in Eq. (19) (Thommes et al. 2015).

$$\frac{\frac{p}{p^{\circ}}}{n\left(1-\frac{p}{p^{\circ}}\right)}=\frac{1}{n_m C}+\frac{C-1}{n_m C}\left(\frac{p}{p^{\circ}}\right) \tag{19}$$

Where; n is the specific amount adsorbed, p/p° is the relative pressure, n_m is the specific monolayer capacity.

Even with the theoretical deficiencies BET theory is used for determining the specific surface area of the adsorbents (BET surface area) (Ościk 1982). The BET specific area is calculated with Eq. (20).

$$a_s(BET)=n_m L\frac{\sigma_m}{m} \tag{20}$$

Where σ_m is the molecular cross-sectional area.

Surface area, pore size and pore volume can be measured with the analysis.

6.3.3 XRD

XRD analysis is executed with 2° to 70° 2θ. X-ray diffraction was performed using a PANalytical Empyrean 3 diffractometer (Cu tube, λ = 0.15406 nm) equipped with poly-capillary optics (slit controlled beam size with height of 1 mm and width of 8 mm), a PIXcel3D-Medipix3 detector (operated in scanning line detector mode), and a Si zero background powder holder. The used tube settings were 30 kV voltage and 30 mA current.

7 Results and discussion

The SEM results presented in Figure 9 indicate that the synthesis is partially succeeded but some starting chemicals remain. The material is not very homogeneous and taller and narrower particles can be observed that differ from the shorter tubes that are MFM-300(Al).

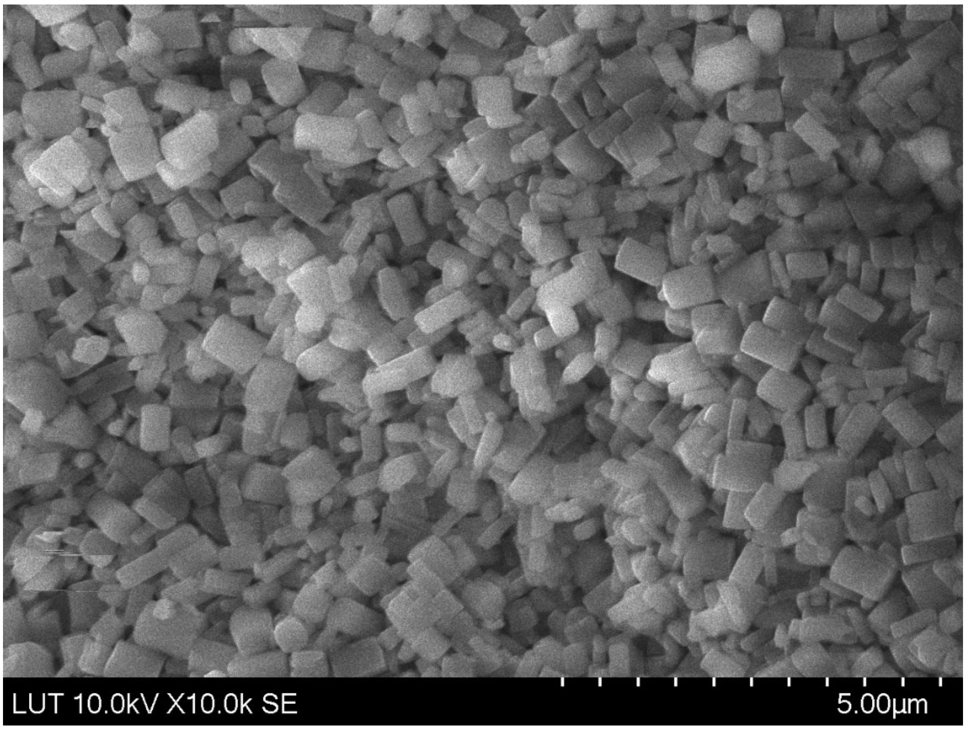

Figure 9. SEM picture of MFM-300(Al)

As seen in Figure 9 the particles are approximately 1 µm long and 0.5 µm wide. The EDS results are presented in Table 12.

Table 12. The results of EDS analysis

Elements	Weight %
Carbon, C	50.36
Oxygen, O	43.19
Aluminium, Al	6.45

As seen in Table 12 most of the atoms in the surface of the material is carbon and oxygen. There is also some aluminium. EDS analysis does not present the hydrogen atoms.

The same results can be obtained from the XRD figure (Figure 10). While most of the peaks indicate the material for MFM-300(Al) the peak at 20° as well as the first peak at ~25° are shorter than in the reference (Thomas-Hillman et al. 2019).

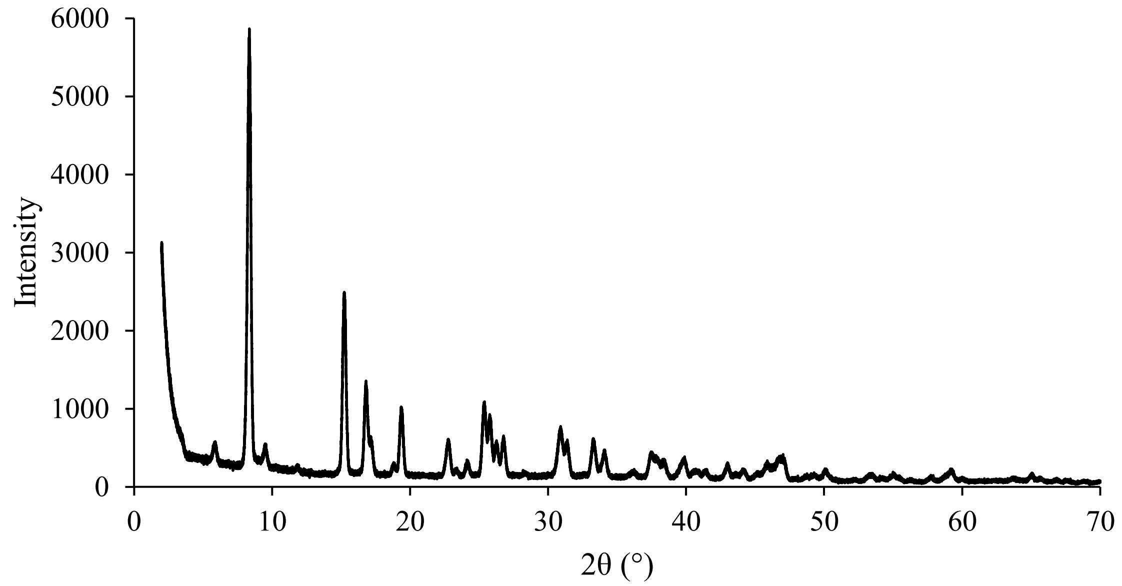

Figure 10. XRD spectra from the MFM-300(Al) MOF sample

The obtained BET surface area is 145.68 m^2/g which is significantly lower than the ~1000 m^2/g found in literature which supports the conclusion of MOF synthesis chemicals remaining in the sample. The adsorption and desorption isotherms obtained from the BET analysis is presented in Figure 11.

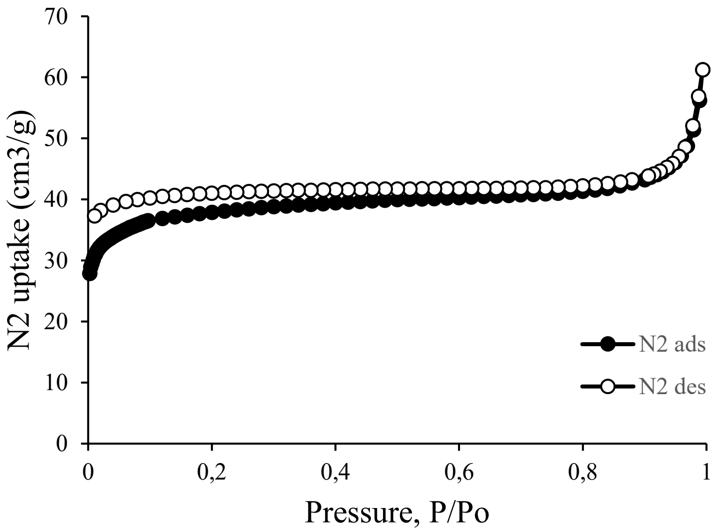

Figure 11. Adsorption and desorption isotherms of MFM-300(Al) MOF using pure N_2 at 77 K

The adsorption isotherm of SO_2 with MFM-300(Al) as adsorbent is presented in Figure 12 and for NO_2 in Figure 13. The R square and standard error values of the figures are presented in Table 13.

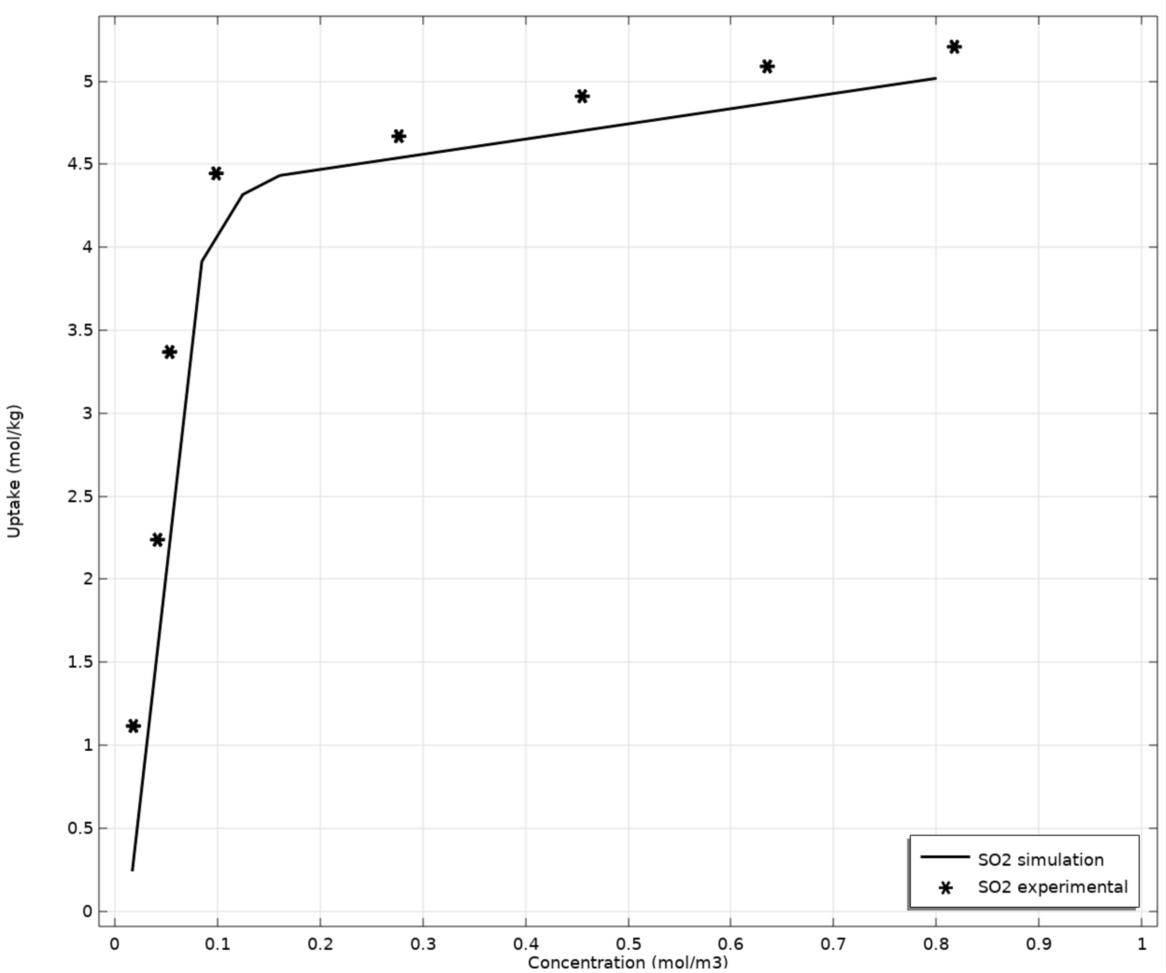

Figure 12. SO_2 adsorption isotherm with MFM-300(Al) as adsorbent in 298.15 K and 1 atm and 60 minutes as experiment time. Experimental data: (Han et al. 2018)

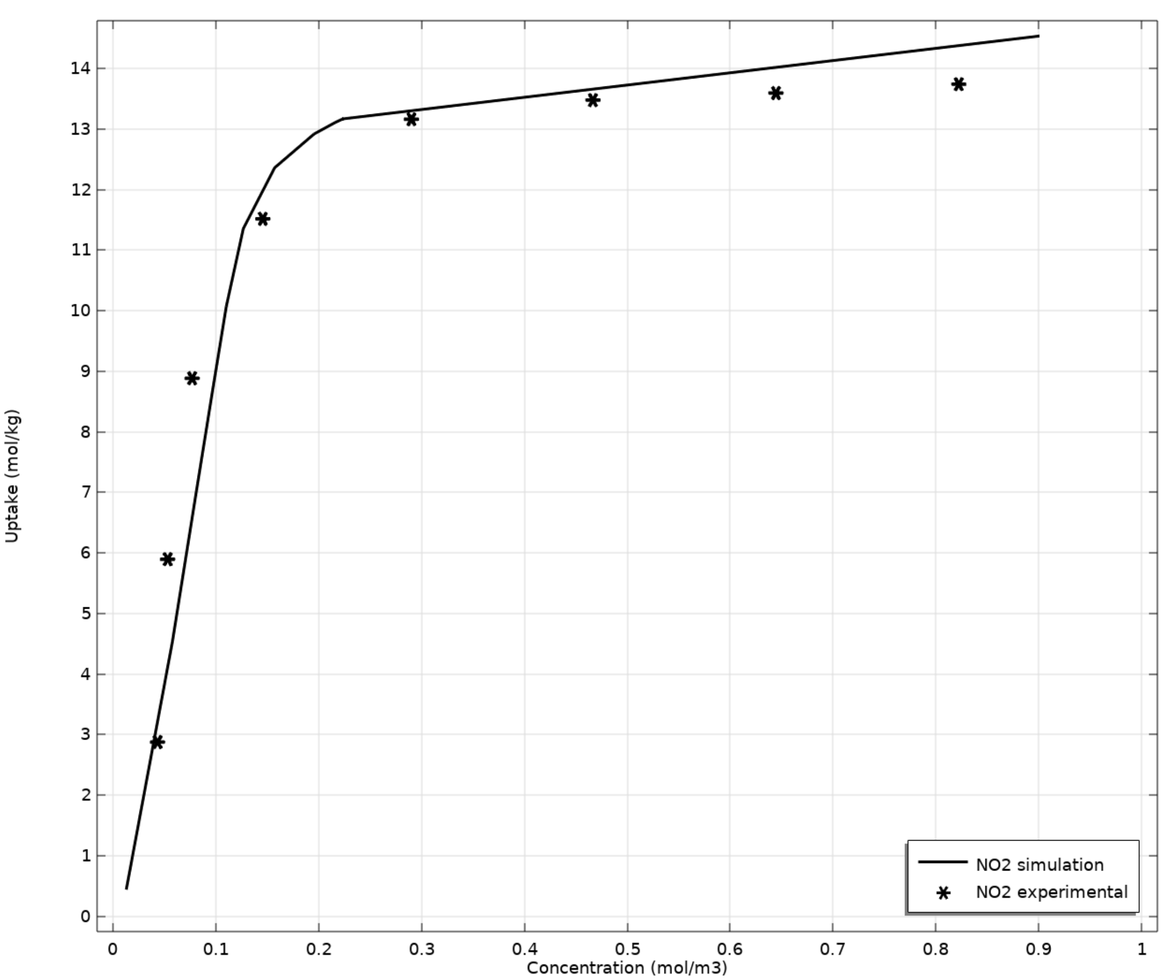

Figure 13. NO_2 adsorption isotherm with MFM-300(Al) as adsorbent in 298.15 K and 1 atm and 120 minutes as experiment time. Experimental data: (Han et al. 2018)

Table 13. R^2 and standard error values of SO_2 and NO_2 adsorption isotherms

	R^2	Standard error
SO_2 adsorption isotherm	0.69	0.14
NO_2 adsorption isotherm	0.74	0.21

When all three isotherms, SO_2, NO_2 and N_2, are plotted in the same figure the results are as in figure 14.

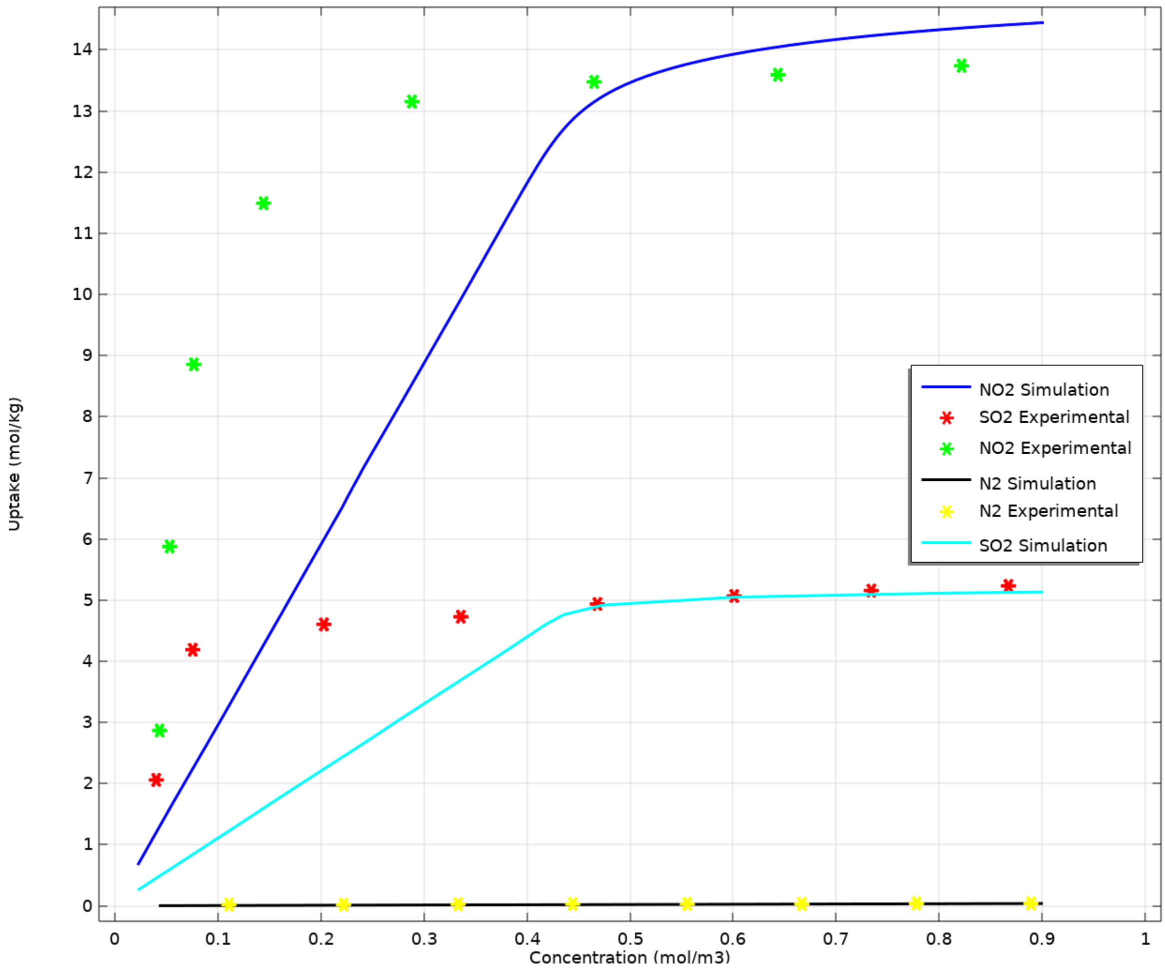

Figure 14. Adsorption isotherms of NO_2, SO_2 and N_2 with MFM-300(Al) as adsorbent in 298.15 K and 1 atm and 10 minutes as experiment time. Experimental data: (Han et al. 2018)

It can be seen from figure 12-14 that in the case of one adsorbed gas the simulation manages to follow the results from the reference but in the case of competitive adsorption of NO2 and SO2 there are some problems. This might be caused by the difficulty for the application to simulate the complex adsorption or because the adsorbent is adsorbing both gases, causing the isotherms of each component to not be as rapid. This might be caused by the simulation not recognising the selectivity for the components and adsorbing each component by equal preference. Barely any N_2 is adsorbed with MFM-300(Al) which is according to the reference.

Adsorbed concentration of SO_2 as a function of time is presented in Figure 15 and the concentration of NO_2 in Figure 16. All three components, SO_2, NO_2 and N_2, adsorbed concentrations as functions of time are presented in Figure 17.

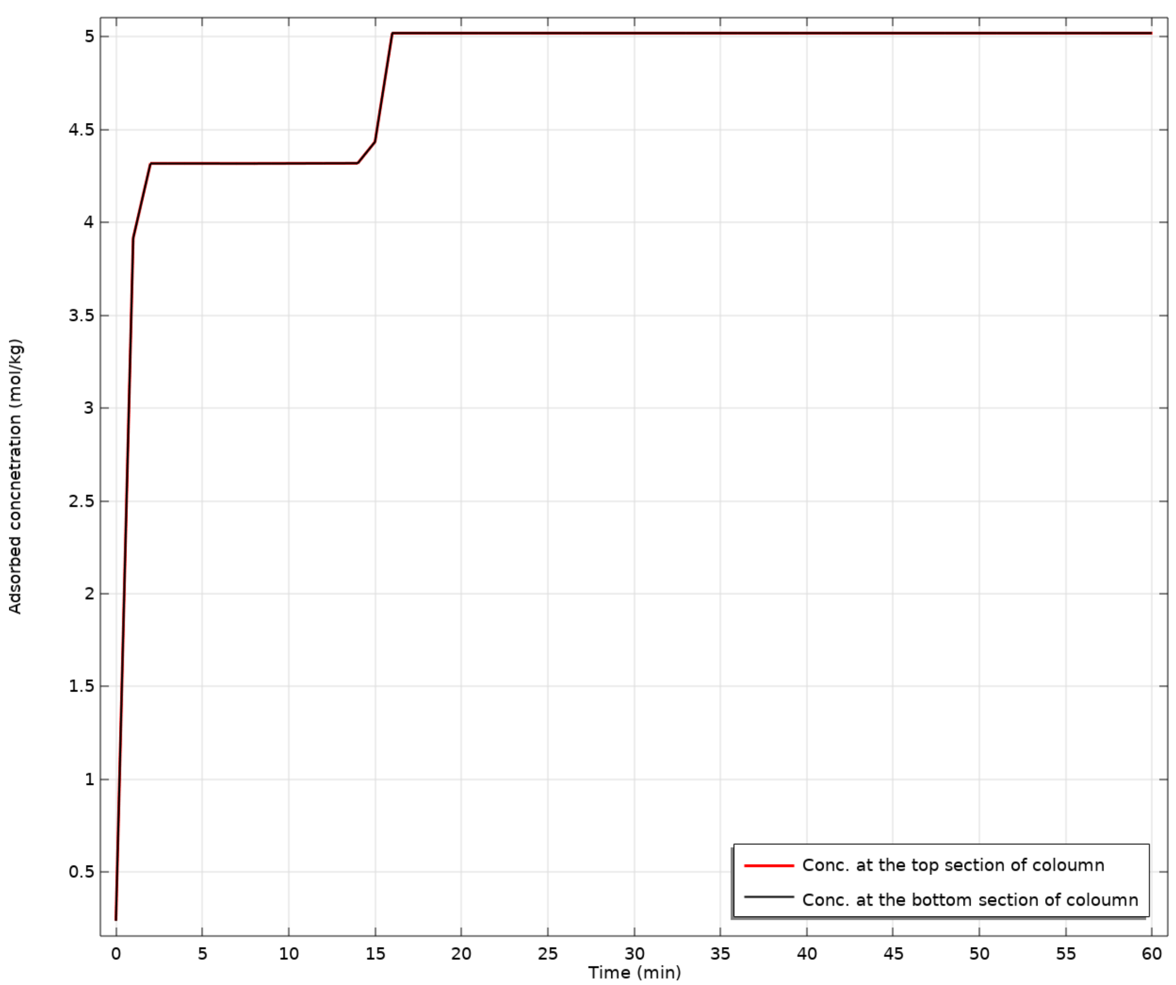

Figure 15. Concentration as a function of time for SO_2 adsorption with MFM-300(Al) as adsorbent

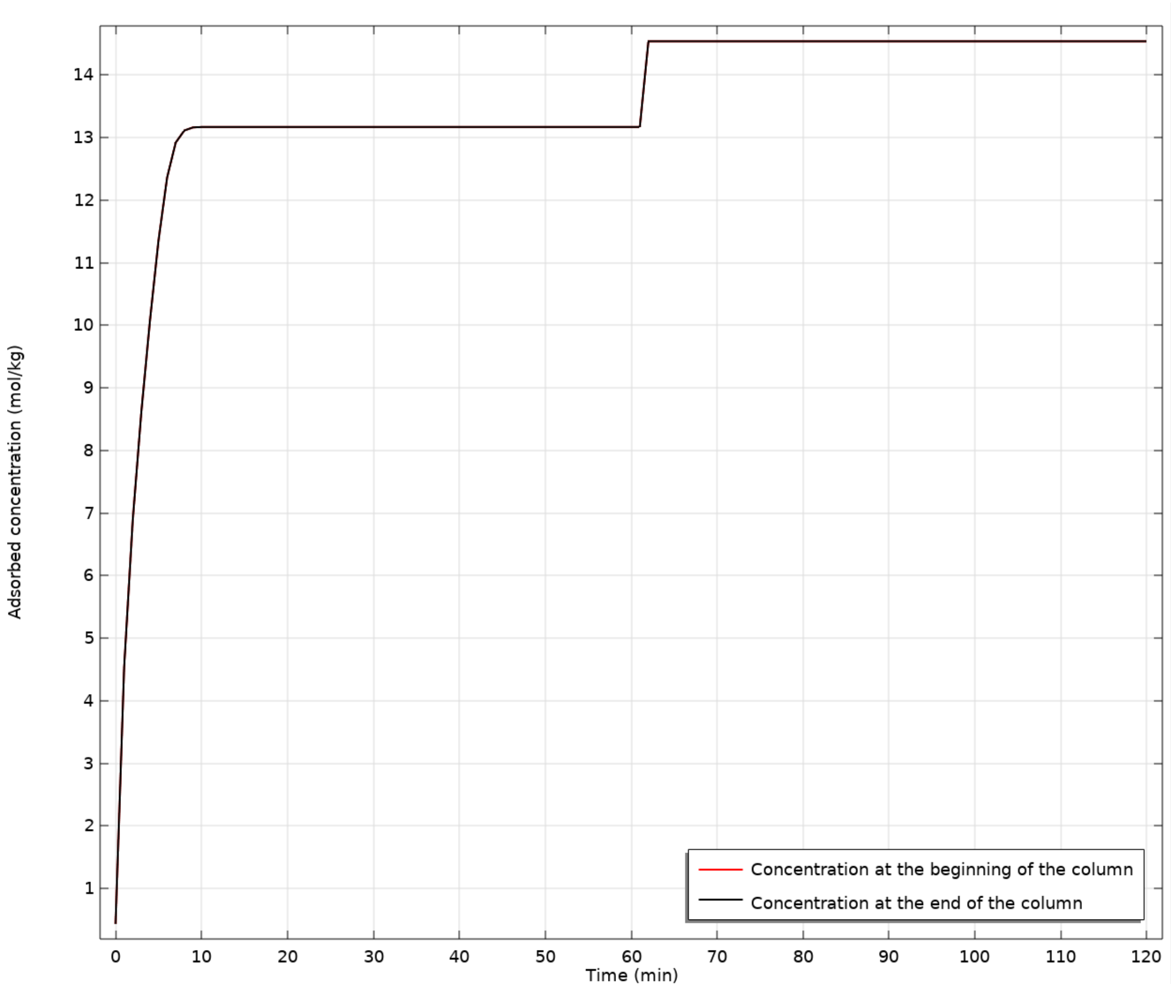

Figure 16. Adsorbed concentration as a function of time for NO_2 adsorption with MFM-300(Al) as an adsorbent

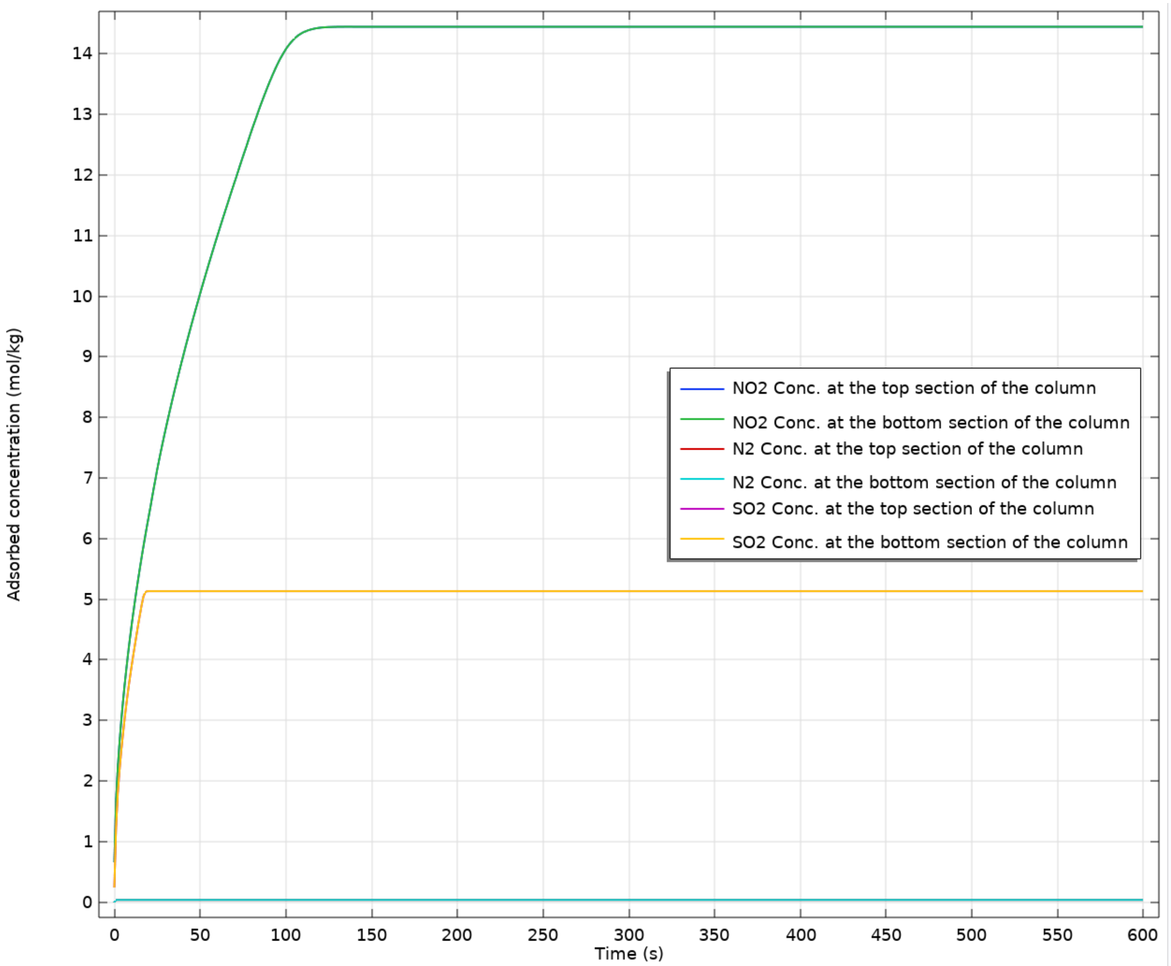

Figure 17. Adsorbed concentration of SO_2, NO_2 and N_2 as a function of time when MFM-300(Al) is used as adsorbent

It can be seen from Figure 15 that the adsorption tests need 16 minutes to complete for SO2 adsorption with MFM-300(Al) and for NO2 (Figure 16) it needs 62 minutes. In that time the adsorbed concentration at the end of the column reaches the maximum adsorbed concentration limit. In the simulation with competitive adsorption the saturation times are much lower, only under two minutes for NO_2 and less than a minute for SO_2. The adsorbed concentration profile in the column at different times NO_2 is presented in Figure 18 and for all three components in Figure 19. The adsorbed concentration profile for SO_2 was behaving strangely in the simulation so that figure is excluded from the thesis.

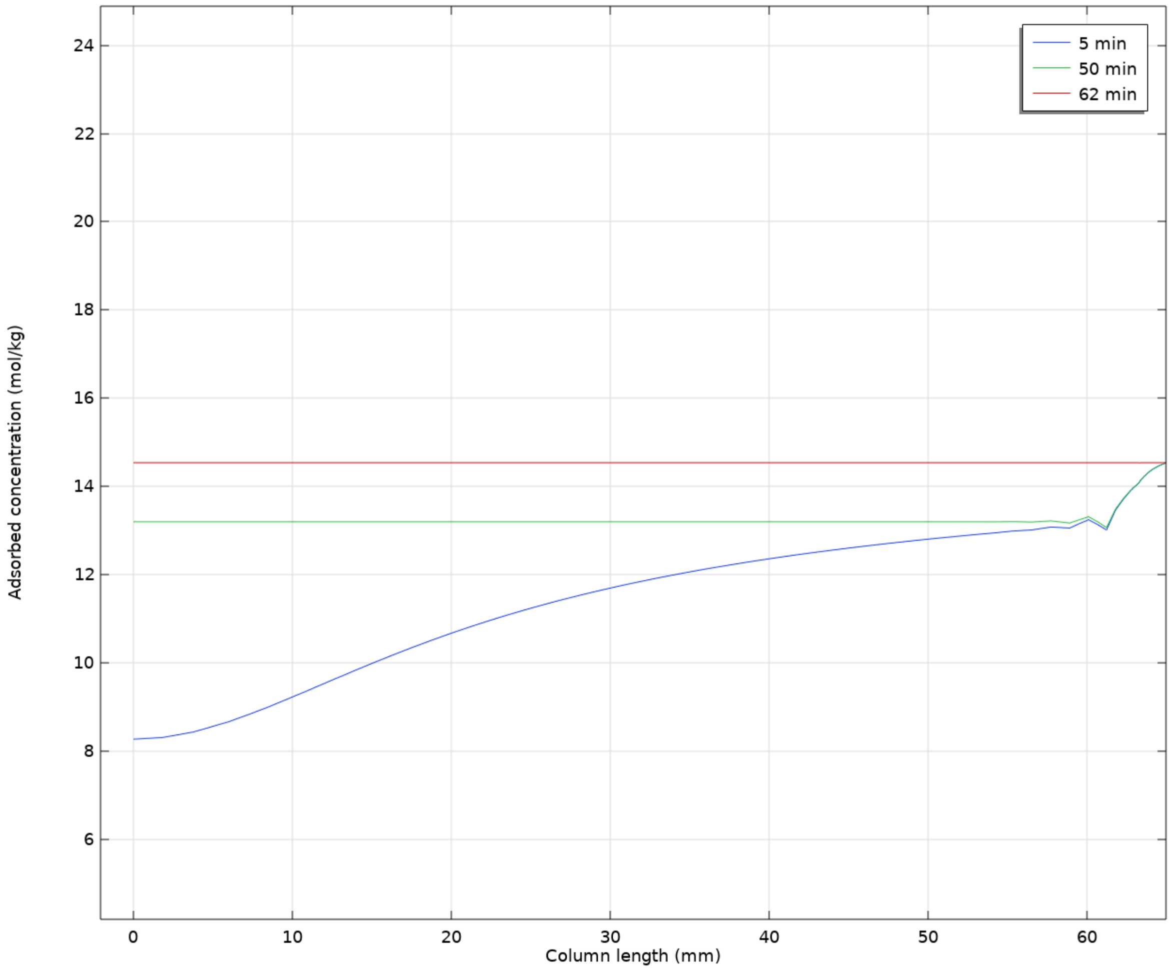

Figure 18. Adsorbed concentration of NO_2 at 5 min, 50 min and 70 min at different column lengths when MFM-300(Al) is used as adsorbent

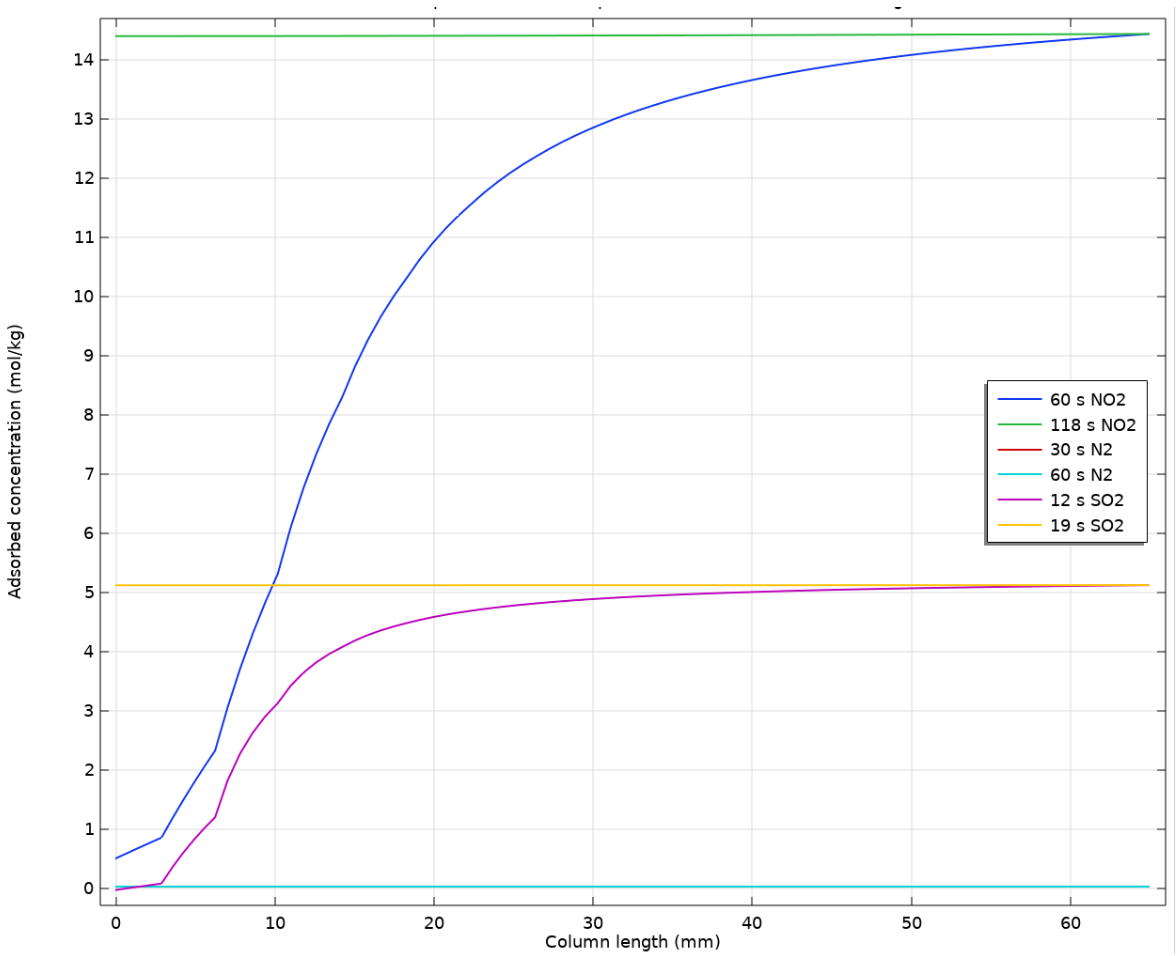

Figure 19. Adsorbed concentration of SO_2, NO_2 and N_2 at before and after saturation at different column lengths when MFM-300(Al) is used as adsorbent

The saturation time for NO_2 adsorption is 62 minutes which can be seen from Figure 18 as well. In Figure 19 the saturation time for NO_2 adsorption is 1 minute and 58 seconds and for SO_2 it is 19 seconds. The saturation times from Figure 19 are too short and don't match the experiment times used in previous adsorption experiments with MFM-300(Al).

8 Conclusions

The current methods for air pollution removal are not sufficient since about 7 million deaths are annually linked to air quality. Even in Finland, where air quality is in top class on global comparison, approximately 1500 deaths can be linked to air pollution every year. Metal organic frameworks show great potential for the removal of these harmful gases such as SO_2 and NO_2.

SO_2 can be adsorbed with several different MOFs very effectively. The best results can be achieved with MIL-101(Cr)-4F(1%), MFM-170, SIFSIX-1-Cu, MFM-300(Al) and MIL-160. All these materials show great stability, selectivity, and adsorption capacity values. For the removal of NO_2 the options are more limited due to the corrosive nature of the gas. UiO-66-NH_2, MFM-300(Al), Cu-BTC and Mg-MOF-74 can all be employed in the adsorption of NO_2, but the most outstanding results are obtained with MFM-300(Al).

MFM-300(Al) is chosen for this thesis because it remains its stability and shows great adsorption capacity as well as selectivity for SO_2 and NO_2. The material has high thermal stability and is stable in dry and humid conditions. While having great adsorption capacity values for NO_2 and SO_2, it adsorbs significantly less CO_2 and minimal amount of N_2 which both are harmless and highly abundant in typical flue gas.

The synthesis of MFM-300(Al) is relatively sustainable. With the microwave assisted synthesis, the synthesis time is only 10 minutes, which is very short reaction time compared to many other syntheses, and the autoclave synthesis method of MFM-300(Al) which takes three days. It doesn't require any harmful chemicals as it only needs H4BPTC and $AlCl_3 \cdot 6 H_2O$ to produce the material. However, with the synthesis conditions presented in this thesis the results obtained are not optimal and some changes are required.

The simulation results show that great adsorption capacity values for SO_2 and NO_2 can be achieved with MFM-300(Al) while adsorbing minimal values of N_2. Some issues remain in the simulation, such as the very short saturation times obtained from the simulation with competitive adsorption. The simulations with only pure gases show more realistic results and don't have the problem of selectivity and preferential adsorption. The adsorption isotherms fit the experimental results from the reference relatively well with R^2 values of 0.69 and 0.74 for SO_2 and NO_2, respectively. The saturation time for NO_2 adsorption is 62 minutes and for SO_2 adsorption 16 minutes. However, there are some issues with the pure gas simulations as well since the adsorbed concentration/column length figure of SO_2 was behaving strangely.

In conclusion, MFM-300(Al) is an interesting and promising material for toxic gas removal. The sustainable synthesis and potential for very high adsorption capacity values and great selectivity for SO_2 and NO_2 over CO_2 and N_2 give a reason to continue researching the possibilities of MFM-300(Al) as an adsorbent.

References

Arsie, I.; D'Aniello, F.; Pianese, C.; De Cesare, M. et al. Development and Experimental Validation of a Control Oriented Model of SCR for Automotive Application. SAE Technical Paper. 2018.Vol.1(1263). ISSN: 0148-7191

Asghar, Usama; Rafiq, Sikander; Anwar, Adeel; Iqbal, Tanveer; Ahmed, Ashfaq; Jamil, Farrukh; Khurram, M. Shahzad; Akbar, Majid Majeed; Farooq, Abid; Shah, Noor S.; Park, Young-Kwon. Review on the progress in emission control technologies for the abatement of CO2, SOx and NOx from fuel combustion. Journal of Environmental Chemical Engineering. 2021. Vol.9 (5). p.106064. ISSN: 2213-3437.

Brandt, Philipp; Nuhnen, Alexander; Lange, Marcus; Möllmer, Jens; Weingart, Oliver; Janiak, Christoph. Metal–Organic Frameworks with Potential Application for SO_2 Separation and Flue Gas Desulfurization. ACS Applied Materials & Interfaces. 2019. Vol.11 (19). p.17350-17358. ISSN: 1944-8244

Carter, Joseph H; Morris, Christopher G; Godfrey, Harry G. W; Day, Sarah J; Potter, Jonathan; Thompson, Stephen P; Tang, Chiu C; Yang, Sihai; Schröder, Martin. 2020. ACS Applied Materials & Interfaces. Vol.12 (38). p.42949-42954. ISSN: 1944-8244.

Çelik, P. A.; Aksoy, D. Ö.; Koca, S.;Koca, H.; Çabuk, A. The approach of biodesulfurization for clean coal technologies: a review. International Journal of Environmental Science and Technology. 2019. Vol.16(4). pp. 2115-2132. ISSN: 1735-1472.

Cordoba, Patricia. Status of Flue Gas Desulphurisation (FGD) systems from coal-fired power plants: Overview of the physic-chemical control processes of wet limestone FGDs. Fuel (Guildford). 2015. Vol.144. p.274-286. ISSN: 0016-2361.

Cui, Xili; Yang, Qiwei; Yang, Lifeng; Krishna, Rajamani; Zhang, Zhiguo; Bao, Zongbi; Wu, Hui; Ren, Qilong; Zhou, Wei; Chen, Banglin; Xing, Huabin. Ultrahigh and Selective SO_2 Uptake in Inorganic Anion-Pillared Hybrid Porous Materials. Advanced materials (Weinheim). 2017. Vol.29 (28). p. n/a. ISSN: 0935-9648.

Daglar, Hilal; Altintas, Cigdem; Erucar, Ilknur; Heidari, Golnaz; Zare, Ehsan Nazarzadeh; Moradi, Omid; Srivastava, Varsha; Iftekhar, Sidra; Keskin, Seda; Sillanpää, Mika. 2022.

Metal-organic framework-based materials for the abatement of air pollution and decontamination of wastewater. Chemosphere (Oxford). Vol.303(2). p.135082-135082. ISSN: 0045-6535.

Gascon, Jorge; Corma, Avelino; Kapteijn, Freek; Llabrés i Xamena, Francesc X. 2014. Metal Organic Framework Catalysis: Quo vadis? ACS Catalysis. Vol.4 (2). p.361-378. ISSN: 2155-5435.

Grant Glover, T.; Peterson, Gregory W.; Schindler, Bryan J.; Britt, David; Yaghi, Omar. MOF-74 building unit has a direct impact on toxic gas adsorption. Chemical Engineering Science. 2011. Vol.66 (2). p.163-170. ISSN: 0009-2509.

Han, Xue; Yang, Sihai; Schröder, Martin. Porous metal–organic frameworks as emerging sorbents for clean air. Nature reviews. Chemistry. 2019. Vol.3 (2). p.108-118. ISSN: 2397-3358.

Han, Xue; Godfrey, Harry G W; Briggs, Lydia; Davies, Andrew J; Cheng, Yongqiang; Daemen, Luke L; Sheveleva, Alena M; Tuna, Floriana; McInnes, Eric J L; Sun, Junliang; Drathen, Christina; George, Michael W; Ramirez-Cuesta, Anibal J; Thomas, K Mark; Yang, Sihai; Schröder, Martin. Reversible adsorption of nitrogen dioxide within a robust porous metal-organic framework. Nature Materials. 2018. Vol.17 (8). p.691-696. ISSN: 1476-1122.

Healy, Colm; Patil, Komal M.; Wilson, Benjamin H.; Hermanspahn, Lily; Harvey-Reid, Nathan C.; Howard, Ben I.; Kleinjan, Carline; Kolien, James; Payet, Fabian; Telfer, Shane G.; Kruger, Paul E.; Bennett, Thomas D. 2020. The thermal stability of metal-organic frameworks. Coordination Chemistry Reviews. Vol.419. p.213388. ISSN: 0010-8545

Hendon, Christopher H; Rieth, Adam J; Korzyński, Maciej D; Dincă, Mircea. 2017. Grand Challenges and Future Opportunities for Metal–Organic Frameworks. ACS Central Science. Vol.3 (6). p.554-563. ISSN: 2374-7943.

Henkelis, Susan E; Judge, Patrick T; Hayes, Sophia E; Nenoff, Tina M. Preferential SOx Adsorption in Mg-MOF-74 from a Humid Acid Gas Stream. ACS Applied Materials & Interfaces. 2021. Vol.13 (6). p.7278-7284. EISSN: 1944-8252.

Ilmatieteenlaitos. Ilmansaasteet. [Online document]. [Accessed 9.2.2023]. Available: https://www.ilmatieteenlaitos.fi/ilmansaasteet

Jurado-Vázquez, Tamara; Sánchez-González, Elí; Campos-Reales-Pineda, Alberto E.; Islas-Jácome, Alejandro; Lima, Enrique; González-Zamora, Eduardo; Ibarra, Ilich A. 2019. MFM-300: From air pollution remediation to toxic gas detection. Polyhedron. Vol.157. p.495-504. ISSN: 0277-5387.

Kim, Ki Chul. Design strategies for metal-organic frameworks selectively capturing harmful gases. Journal of Organometallic Chemistry. 2018. Vol.854. p.94-105. ISSN: 0022-328X.

Kumar, K. Vasanth; Gadipelli, Srinivas; Wood, Barbara; Ramisetty, Kiran A; Stewart, Andrew A; Howard, Christopher A; Brett, Dan J. L; Rodriguez-Reinoso, F. 2019. Characterization of the adsorption site energies and heterogeneous surfaces of porous materials. Journal of materials chemistry. A, Materials For Energy and Sustainability. Vol.7 (17). p.114-1137. ISSN: 2050-7488

Levasseur, Benoit; Petit, Camille; Bandosz, Teresa J. 2010. Reactive Adsorption of NO_2 on Copper-Based Metal−Organic Framework and Graphite Oxide/Metal−Organic Framework Composites. ACS Applied Materials & Interfaces. Vol.2 (12). p.3606-3613. ISSN: 1944-8244.

Li, Yingwei; Yang, Ralph T. 2007. Gas Adsorption and Storage in Metal−Organic Framework MOF-177. Langmuir. Vol.23 (26). p.12937-12944. ISSN: 0743-7463.

Lima, Eder C.; Gomes, Adriano A.; Tran, Hai Nguyen. 2020. Comparison of the nonlinear and linear forms of the van't Hoff equation for calculation of adsorption thermodynamic parameters ($\Delta S°$ and $\Delta H°$). Journal of Molecular Liquids. Vol.311. p.113315. ISSN: 0167-7322.

Liu, Jia-Xiang; Li, Jie; Tao, Wen-Quan; Li, Zhuo. 2021. 3.Al-Based Metal-Organic Framework MFM-300 and MIL-160 for SO2 Capture: A Molecular Simulation Study. Fluid Phase Equilibria. Vol.536. p.112963. ISSN: 0378-3812.

Liu, Yangyang; Howarth, Ashlee J.; Hupp, Joseph T.; Farha, Omar K. 2015. Selective Photooxidation of a Mustard-Gas Simulant Catalyzed by a Porphyrinic Metal-Organic Framework. Angewandte Chemie (International ed.). Vol.54 (31). p.9001-9005. ISSN: 1433-7851.

Mart´ınez-Ahumada, Eva; D´ıaz-Ram´ırez, Mariana L.; de J. Velasquez-Hernandez, Miriam; Jancik, Vojtech; Ibarra, Ilich A. Capture of toxic gases in MOFs: SO_2, H2S, NH3 and NOx. Chem. Sci. 2021. Vol.12. ISSN: 6772-6799.

Martínez-Ahumada, Eva; Díaz-Ramírez, Mariana L; Lara-García, Hugo A; Williams, Daryl R; Martis, Vladimir; Jancik, Vojtech; Lima, Enrique; Ibarra, Ilich A. High and reversible SO capture by a chemically stable Cr()-based MOF. Journal of materials chemistry. A, Materials for Energy and Sustainability. 2020. Vol.8 (23). p.11515-1152. ISSN: 2050-7488.

Nguyen, Duc Ba; Nguyen, Van Toan; Heo, Il Jeong; Mok, Young Sun. 2019. Removal of NOx by selective catalytic reduction coupled with plasma under temperature fluctuation condition. Journal of Industrial and Engineering Chemistry. Vol.72(0). pp.400-407. ISSN: 1226-086X.

OECD. 2013. Sulphur oxides (SOx) and nitrogen oxides (NOx) emissions. Environment at a Glance 2013: OECD Indicators. OECD Publishing, Paris. https://doi.org/10.1787/9789264185715-7-en

Ościk, J. 1982. Adsorption. Chichester; New York: Horwood: Halsted Press. 206 p. ISBN: 0-85312-166-4

Pacciani, R; Torres, J; Solsona, P; Coe, C; Quinn, R; Hufton, J; Golden, T; Vega, L. F. Influence of the Concentration of CO2 and SO_2 on the Absorption of CO2 by a Lithium Orthosilicate-Based Absorbent. Environmental Science & Technology. 2011. Vol.45 (16). p.7083-7088. ISSN: 0013-936X.

Permyakova, Anastasia; Skrylnyk, Oleksandr; Courbon, Emilie; Affram, Maame; Wang, Sujing; Lee, U-Hwang; Valekar, Anil H.; Nouar, Farid; Mouchaham, Georges; Devic, Thomas; De Weireld, Guy; Chang, Jong-San; Steunou, Nathalie; Frère, Marc; Serre, Christian. 2017. Synthesis Optimization, Shaping, and Heat Reallocation Evaluation of the Hydrophilic Metal–Organic Framework MIL-160(Al). ChemSusChem. Vol.10 (7). p.1419-1426. ISSN: 1864-5631.

Peterson, Gregory W.; Mahle, John J.; DeCoste, Jared B.; Gordon, Wesley O.; Rossin, Joseph A. 2016. Extraordinary NO2 Removal by the Metal-Organic Framework UiO-66-NH2. Angewandte Chemie (International ed.). Vol.55 (21). p.6235-6238. ISSN: 1433-7851.

Rodriguez, José A; Jirsak, Tomas. 2000. Chemistry of NO2 on CeO_2 and MgO: Experimental and theoretical studies on the formation of NO_3. J. Chem. Phys. Vol.112(9929). DOI: https://doi.org/10.1063/1.481629

Savage, Mathew; Cheng, Yongqiang; Easun, Timothy L.; Eyley, Jennifer E.; Argent, Stephen P.; Warren, Mark R.; Lewis, William; Murray, Claire; Tang, Chiu C.; Frogley, Mark D.; Cinque, Gianfelice; Sun, Junliang; Rudić, Svemir; Murden, Richard T.; Benham, Michael J.; Fitch, Andrew N.; Blake, Alexander J.; Ramirez-Cuesta, Anibal J.; Yang, Sihai; Schröder, Martin. Selective Adsorption of Sulfur Dioxide in a Robust Metal-Organic Framework Material. Advanced Materials (Weinheim). 2016. Vol.28 (39). p.8705-8711. ISSN: 0935-9648.

Scala, Fabrizio ; Lancia, Amedeo ; Nigro, Roberto ; Volpicelli, Gennaro. 2005. Spray-Dry Desulfurization of Flue Gas from Heavy Oil Combustion. Journal of the Air & Waste Management Association. Vol.55 (1). p.20-29. ISSN: 1096-2247.

Smith, Gemma L; Eyley, Jennifer E; Han, Xue; Zhang, Xinran; Li, Jiangnan; Jacques, Nicholas M; Godfrey, Harry G W; Argent, Stephen P; McCormick McPherson, Laura J; Teat, Simon J; Cheng, Yongqiang; Frogley, Mark D; Cinque, Gianfelice; Day, Sarah J; Tang, Chiu C; Easun, Timothy L; Rudić, Svemir; Ramirez-Cuesta, Anibal J; Yang, Sihai; Schröder, Martin. Reversible coordinative binding and separation of sulfur dioxide in a robust metal-organic framework with open copper sites. Nature Materials. 2019. Vol.18 (12). p.1358-1365. ISSN: 1476-1122.

Song, Xue-Dan; Wang, Se; Hao, Ce; Qiu, Jie-Shan. 2014. Investigation of SO_2 gas adsorption in metal–organic frameworks by molecular simulation. Inorganic Chemistry Communications. Vol.46. p.277-281. ISSN: 1387-7003.

Subcommittee on Acute Exposure Guideline Levels. Acute exposure guideline levels for selected airborne chemicals. Washington, D.C.: National Academy Press. ISBN: 0-309-18354-5.

Sun, Weizhen; Lin, Li-Chiang; Peng, Xuan; Smit, Berend. Computational screening of porous metal-organic frameworks and zeolites for the removal of SO_2 and NOx from flue gases. AIChE Journal. 2014. Vol.60 (6). p.2314-2323. ISSN: 0001-1541.

Suo, Xian; Yu, Ying; Qian, Siheng; Zhou, Lin; Cui, Xili; Xing, Huabin. Tailoring the Pore Size and Chemistry of Ionic Ultramicroporous Polymers for Trace Sulfur Dioxide Capture with High Capacity and Selectivity. Angewandte Chemie. 2021. Vol.133 (13). p.7062-7067. ISSN: 0044-8249.

Stock, Norbert; Biswas, Shyam. 2012. Synthesis of Metal-Organic Frameworks (MOFs): Routes to Various MOF Topologies, Morphologies, and Composites. Chemical Reviews. Vol.112 (2). p.933-969. ISSN: 0009-2665.

Tan, Kui; Zuluaga, Sebastian; Wang, Hao; Canepa, Pieremanuele; Soliman, Karim; Cure, Jeremy; Li, Jing; Thonhauser, Timo; Chabal, Yves J. 2017. Interaction of Acid Gases SO_2 and NO2 with Coordinatively Unsaturated Metal Organic Frameworks: M-MOF-74 (M = Zn, Mg, Ni, Co). Chemistry of Materials. Vol.29 (10). p.4227-4235. ISSN: 0897-4756.

Thomas-Hillman, Ieuan; Stevens, Lee A; Lange, Marcus; Möllmer, Jens; Lewis, William; Dodds, Chris; Kingman, Samuel W; Laybourn, Andrea. 2019. Developing a sustainable route to environmentally relevant metal-organic frameworks: ultra-rapid synthesis of MFM-300(Al) using microwave heating. Green Chemistry: an International Journal and Green Chemistry Resource: GC. Vol.21 (18). p.539-545. ISSN: 1463-9262.

Thommes, Matthias; Kaneko, Katsumi; Neimark, Alexander V.; Olivier, James P.; Rodriguez-Reinoso, Francisco; Rouquerol, Jean; Sing, Kenneth S.W. 2015. Physisorption of gases, with special reference to the evaluation of surface area and pore size distribution (IUPAC Technical Report). Pure and Applied Chemistry. Vol.87 (9). p.1051-1069. ISSN: 0033-4545.

Vestenius, Mika. 2016. Liikenne ja puunpoltto aiheuttavat edelleen ilmanlaatuongelmia Suomessa. Ilmatieteenlaitos. [Online document]. [Accessed 14.2.2023]. Available: https://www.ilmatieteenlaitos.fi/tiedote/286500336

Wang, H.; Bai, J.Q.; Yin, Y.; Wang, S.F. 2020. Experimental and numerical study of SO_2 removal from a CO_2/SO_2 gas mixture in a Cu-BTC metal organic framework. Journal of Molecular Graphics & Modelling. Vol.96. p.107533-107533. ISSN: 1093-3263.

WHO global air quality guidelines. Particulate matter (PM2.5 and PM10), ozone, nitrogen dioxide, sulfur dioxide and carbon monoxide. Geneva: World Health Organization. ISBN 978-92-4-003422-8.

WHO. 2014. 7 million premature deaths annually linked to air pollution. [Online document]. [Accessed 1.3.2023]. Available: https://www.who.int/news/item/25-03-2014-7-million-premature-deaths-annually-linked-to-air-pollution

Wu, Zhonghua; Wei, Shuxian; Wang, Maohuai; Zhou, Sainan; Wang, Jiahui; Wang, Zhaojie; Guo, Wenyue; Lu, Xiaoqing. 2018. CO2 capture and separation over N2 and CH4 in nanoporous MFM-300(In, Al, Ga, and In-3N): Insight from GCMC simulations. Journal of CO2 Utilization. Vol.28. p.145-151. ISSN: 2212-9820.

Xiang, Wenlong; Zhang, Yueping; Chen, Yifei; Liu, Chang-jun; Tu, Xin. Synthesis, characterization and application of defective metal-organic frameworks: current status and perspectives. Journal of materials chemistry. A, Materials for Energy and Sustainability, 2020. Vol.8 (41). p.21526-21546. ISSN: 2050-7488.

Xue, Zhipeng; Chen, Hao; Zhao, Minmin. Combined Removal Of NOx And SO_2 From Flue Gas At Low Temperature. Environmental Protection, Pollution and Treatment. 2018. Vol.53. Pp. 8. DOI: https://doi.org/10.1051/e3sconf/20185304038

Yamamoto, Yuri; Yamamoto, Hashira; Takada, Daichi; Kuroki, Tomoyuki; Fujishima, Hidekatsu; Okubo, Masaaki. Simultaneous Removal of NOx and SOx from Flue Gas of a Glass Melting Furnace using a Combined Ozone Injection and Semi-dry Chemical Process. Ozone: Science & Engineering. 2016. Vol.38 (3). p.211-218. ISSN: 0191-9512.

Yang, Sihai; Sun, Junliang; Ramirez-Cuesta, Anibal J; Callear, Samantha K; David, William I F; Anderson, Daniel P; Newby, Ruth; Blake, Alexander J; Parker, Julia E; Tang, Chiu C; Schröder, Martin. 2012. Selectivity and direct visualization of carbon dioxide and sulfur dioxide in a decorated porous host. Nature chemistry. Vol.4 (11). p.887-894. ISSN: 1755-4330.

Yu, Zhewei; Deschamps, Johnny; Hamon, Lomig; Karikkethu Prabhakaran, Prasanth; Pré, Pascaline. 2017. Hydrogen adsorption and kinetics in MIL-101(Cr) and hybrid activated carbon-MIL-101(Cr) materials. International Journal of Hydrogen Energy. Vol.42 (12). p.8021-8031. ISSN: 0360-3199

Zhang, Pin. Application study of Bio-FGD based on environmental safety during the coal combustion. IOP Conference Series: Earth and Environmental Science. 2018. Vol. 154(1). pp. 012018. DOI: 10.1088/1755-1315/154/1/012018.

Zhang, Xuan; Zheng, Qing-rong; He, Hong-zhou. 2022. Multicomponent adsorptive separation of CO2, CH4, N2, and H2 over M-MOF-74 and AX-21@M-MOF-74 composite adsorbents. Microporous and Mesoporous Materials. Vol.336. p.111899. ISSN: 1387-1811.

Zhang, Yuanyuan; Yuan, Shuai; Feng, Xiao; Li, Haiwei; Zhou, Junwen; Wang, Bo. 2016. Preparation of Nanofibrous Metal–Organic Framework Filters for Efficient Air Pollution Control. Journal of the American Chemical Society, 2016, Vol.138 (18), p.5785-5788. ISSN: 0002-7863.

Zhou, Hong-Cai; Long, Jeffrey R ;Yaghi, Omar M. Introduction to Metal–Organic Frameworks. Chemical Reviews. 2012. Vol.112 (2). p.673-674. ISSN: 0009-2665.